Selective functional inhibition of a tumor-derived p53 mutant by cytosolic chaperones identified using split-YFP in budding yeast

Ashley S. Denney, Andrew D. Weems,[†] and Michael A. McMurray (iD) *

Department of Cell and Developmental Biology, University of Colorado Anschutz Medical Campus, Aurora, CO 80045, USA
[†]Present address: Department of Bioinformatics, UT Southwestern Medical Center, TX 75390, USA.

*Corresponding author: Email: michael.mcmurray@cuanschutz.edu

Abstract

Life requires the oligomerization of individual proteins into higher-order assemblies. In order to form functional oligomers, monomers must adopt appropriate 3D structures. Molecular chaperones transiently bind nascent or misfolded proteins to promote proper folding. Single missense mutations frequently cause disease by perturbing folding despite chaperone engagement. A misfolded mutant capable of oligomerizing with wild-type proteins can dominantly poison oligomer function. We previously found evidence that human-disease-linked mutations in *Saccharomyces cerevisiae* septin proteins slow folding and attract chaperones, resulting in a kinetic delay in oligomerization that prevents the mutant from interfering with wild-type function. Here, we build upon our septin studies to develop a new approach for identifying chaperone interactions in living cells, and use it to expand our understanding of chaperone involvement, kinetic folding delays, and oligomerization in the recessive behavior of tumor-derived mutants of the tumor suppressor p53. We find evidence of increased binding of several cytosolic chaperones to a recessive, misfolding-prone mutant, p53(V272M). Similar to our septin results, chaperone overexpression inhibits the function of p53(V272M) with minimal effect on the wild type. Unlike mutant septins, p53(V272M) is not kinetically delayed under conditions in which it is functional. Instead, it interacts with wild-type p53 but this interaction is temperature sensitive. At high temperatures or upon chaperone overexpression, p53(V272M) is excluded from the nucleus and cannot function or perturb wild-type function. Hsp90 inhibition liberates mutant p53 to enter the nucleus. These findings provide new insights into the effects of missense mutations.

Keywords: p53; septin; mutant; protein folding; molecular chaperone; heat shock protein 90 (Hsp90); bimolecular fluorescence complementation (BiFC); *Saccharomyces cerevisiae*

Introduction

Higher-order protein structures are essential for life. Protein monomers must be synthesized, correctly folded, and efficiently assembled into homo- or hetero-oligomers while avoiding inappropriate interaction with misfolded partners. Quality control at each step is important to ensure these processes are accurate and timely. Molecular chaperones aid quality control by assisting protein folding through cycles of client binding and release. In a survey of nearly 3000 human disease-causing missense mutant proteins ~30% showed increased association with chaperones relative to the wild-type (WT) allele, and this value is likely an underestimate (Sahni *et al.* 2015). Thus although chaperone binding to WT clients promotes client folding to the native state, in the case of misfolded mutants chaperone engagement does not guarantee that release of the client in a form that is competent for function. Although sequestration of grossly misfolded proteins by chaperones is an established mechanism for maintaining cellular fitness (Escusa-Toret *et al.* 2013), the idea that persistent chaperone

engagement may actually interfere with normal protein function has received much less attention.

Septins are highly conserved cytoskeletal proteins whose assembly into hetero-oligomers is important for various cellular processes (Mostowy and Cossart 2012; Woods and Gladfelter 2021). Septins were originally discovered in *Saccharomyces cerevisiae* as temperature-sensitive (TS) mutants (Hartwell 1971). We previously demonstrated that at low temperatures permissive for cellular function many TS septin mutants are kinetically delayed in their folding, and that this delay has consequences for oligomerization when mutant septin monomers compete with WT monomers (Johnson *et al.* 2015), a quality control phenomenon we termed kinetic allele discrimination in oligomerization (KADO; Schaefer *et al.* 2016). Exclusion of the mutant septin from septin hetero-oligomers ensures that the mutant allele is recessive and does not interfere with the function of the WT allele (Johnson *et al.* 2015). We noticed that the excluded mutant persisted in the cytosol complexed with non-septin proteins, which we identified as cytosolic chaperones (Johnson *et al.* 2015).

Deletion of genes encoding some of the same cytosolic chaperones perturbed KADO and allowed TS-mutant septins to incorporate into hetero-oligomers despite the presence of the WT (Johnson *et al.* 2015). Thus chaperone binding to the mutant septin contributed to the kinetic competition between the two alleles.

In the case of a mutant that is nonfunctional at all temperatures, chaperone deletion converted the otherwise recessive mutant septin to a dominant-lethal allele, presumably by allowing the mutant to incorporate into septin hetero-oligomers and "poison" septin function (Johnson *et al.* 2015). Finally, chaperone overexpression inhibited septin function in cells in which only the mutant septin allele was expressed, consistent with a model in which chaperone engagement sequesters the mutant protein and blocks its ability to assemble into functional hetero-oligomers (Johnson *et al.* 2015). One yeast septin mutant subject to KADO carries the same amino acid substitution as a human mutation that blocks septin hetero-oligomerization and prevents septin function in sperm (Kuo *et al.* 2012; Weems *et al.* 2014; Johnson *et al.* 2015). We wanted to understand more about which chaperones bind WT and mutant septins and the extent to which the mechanisms we discovered with mutant yeast septins apply to other disease-linked mutations in oligomeric proteins.

p53 is a transcription factor and tumor suppressor that is mutated in nearly 50% of human tumors (see the IARC p53 Database, http://p53.iarc.fr). WT p53 exists on a precipice of thermostability, where missense substitutions easily push it "over the edge" in terms of its ability to fold, bind DNA and activate transcription (Bullock *et al.* 1997). Tumor-derived p53 mutants vary in conformation and function. In "contact" mutants, DNA binding is specifically abrogated by substitutions in the DNA-binding region without global effects on p53 conformation, whereas in "conformational" mutants the entire DNA-binding domain (DBD) is misfolded. p53 mutants can also be categorized as dominant or recessive in terms of their inhibitory effect on the function of coexpressed WT p53. Although fungi lack p53, yeast has long been an attractive system for characterizing p53 function using reporters whose transcription depends on p53 oligomerization, nuclear localization, and DNA binding (Sharma *et al.* 2016; Billant *et al.* 2017). Yeast-based analysis of tumor-derived missense mutations in the p53 core domain found that most were dominant-negative, loss-of-function alleles (Dearth *et al.* 2007). The remaining one-third failed to interfere with WT function and this recessive class was enriched for TS mutants (Dearth *et al.* 2007). We wondered if, like the recessive TS septin mutants, kinetic delays in folding/oligomerization or persistent chaperone engagement play a role in this class of p53 mutants. Coupled with the absence in yeast of many factors that exert extrinsic regulation on p53 oligomerization and turnover (*e.g.*, MDM2; Di Ventura *et al.* 2008), the high conservation of all major classes of cytosolic chaperones allows us to focus on effects of mutations on p53 folding, chaperone engagement, and transcriptional activation function.

In this study, we set out to determine how chaperone engagement and kinetic delays in folding contribute to the recessive behavior of a TS p53 mutant. Having previously used functional approaches to find chaperone roles in recessive behavior for septin mutants, we first use mutant septins to test a bimolecular fluorescence complementation (BiFC) screening method to visualize chaperone–client interactions in living cells. We then combine BiFC chaperone screening with genetic and pharmacological manipulation of chaperones to gain a mechanistic understanding of the contributions of protein misfolding and cytosolic chaperones to the ability of a tumor-derived p53 mutant to dominantly interfere with WT function.

Materials and methods
Yeast strains, media, plasmids, and genetic manipulations

Yeast strains are listed in Supplementary Table S1 and were manipulated using standard techniques (Amberg *et al.* 2005). Oligonucleotides are listed in Supplementary Table S2 and plasmids along with construction details are listed in Supplementary Table S3. Yeast cells were cultivated in liquid or solid (2% agar) plates of rich or synthetic (Drop Out Mix Minus various ingredients; United States Biological, Salem, MA) medium containing total 2% sugar (glucose, raffinose, or galactose) or 4% sugar (2% each raffinose and galactose), as needed to maintain plasmid selection and induce expression from the *GAL1/10* promoter. The TH5 strain was propagated on rich or synthetic medium with 100 μg/ml dTMP (thymidine monophosphate, TCI America no. TCT0845), or on minimal medium containing essential amino acids adenine, histidine, and methionine . Drop out medium containing 5-fluoro-orotic acid (FOA; United States Biological) was prepared with 50 μg/ml uracil and 0.1% FOA, except for use at 37° where modified to 0.07% FOA at pH 4.6. Radicicol (AdiopGen no. AG-CN2-0021) was dissolved in DMSO to 10 mg/ml. The bacterial strain DH5α (Agilent Technologies, Santa Clara, CA) was used to propagate plasmids.

Genomic or plasmid DNA from yeast was isolated by resuspending cells in 250 μl of P1 (50 mM Tris-HCl, pH 8.0, 10 mM EDTA, 100 μg/ml RNAse A), adding 0.5-mm glass beads to displace an additional ∼250 μl of volume, and vortexing for 3 min before addition of 250 μl P2 (200 mM NaOH, 1% SDS) and 350 μl N3 (4.2 M guanidine-HCl, 0.9 M potassium acetate, pH 4.8). Lysates were clarified by centrifugation and applied to Zyppy plasmid DNA Miniprep columns (Zymo Research) and DNA was washed and eluted according to the manufacturer's instructions. Alternatively, DNA was precipitated from clarified lysates using sodium acetate and ethanol (Green and Sambrook 2016). Yeast transformation was performed using Frozen-EZ Yeast Transformation Kit II (Zymo Research, Irvine, CA). Bacterial transformation was performed using CaCl$_2$-prepared competent bacterial cells. PCR was performed with Phusion or Q5 high-fidelity polymerase (New England Biolabs, Ipswich, MA) according to the manufacturer's instructions. Site-directed mutagenesis was performed by Keyclone Technologies (San Marcos, CA).

Microscopy

All micrographs were captured with an EVOSfl (Advanced Microscopy Group, Bothell, WA) all-in-one microscope equipped with an Olympus (Tokyo, Japan) 60× oil immersion objective and yellow fluorescent protein (YFP), Texas Red, and GFP filters. Cells from mid to late log cultures were either taken directly from liquid cultures, applied to glass slides and covered with a coverslip, or concentrated by centrifugation, spotted to agarose pads, and covered with a coverslip. For septin microscopy, LED intensity was 100% and exposure times ranged from 500 to 1500 ms. For p53 microscopy, LED intensity for YFP and Texas Red ranged from 80% to 100%, and exposure time ranged from 1000 to 2500 ms, together chosen to produce no more than 10% saturated signal. GFP imaging used 20–30% LED intensity and 30–60 ms exposure. For comparison of samples in an experiment all samples were analyzed using the same intensity and exposure time.
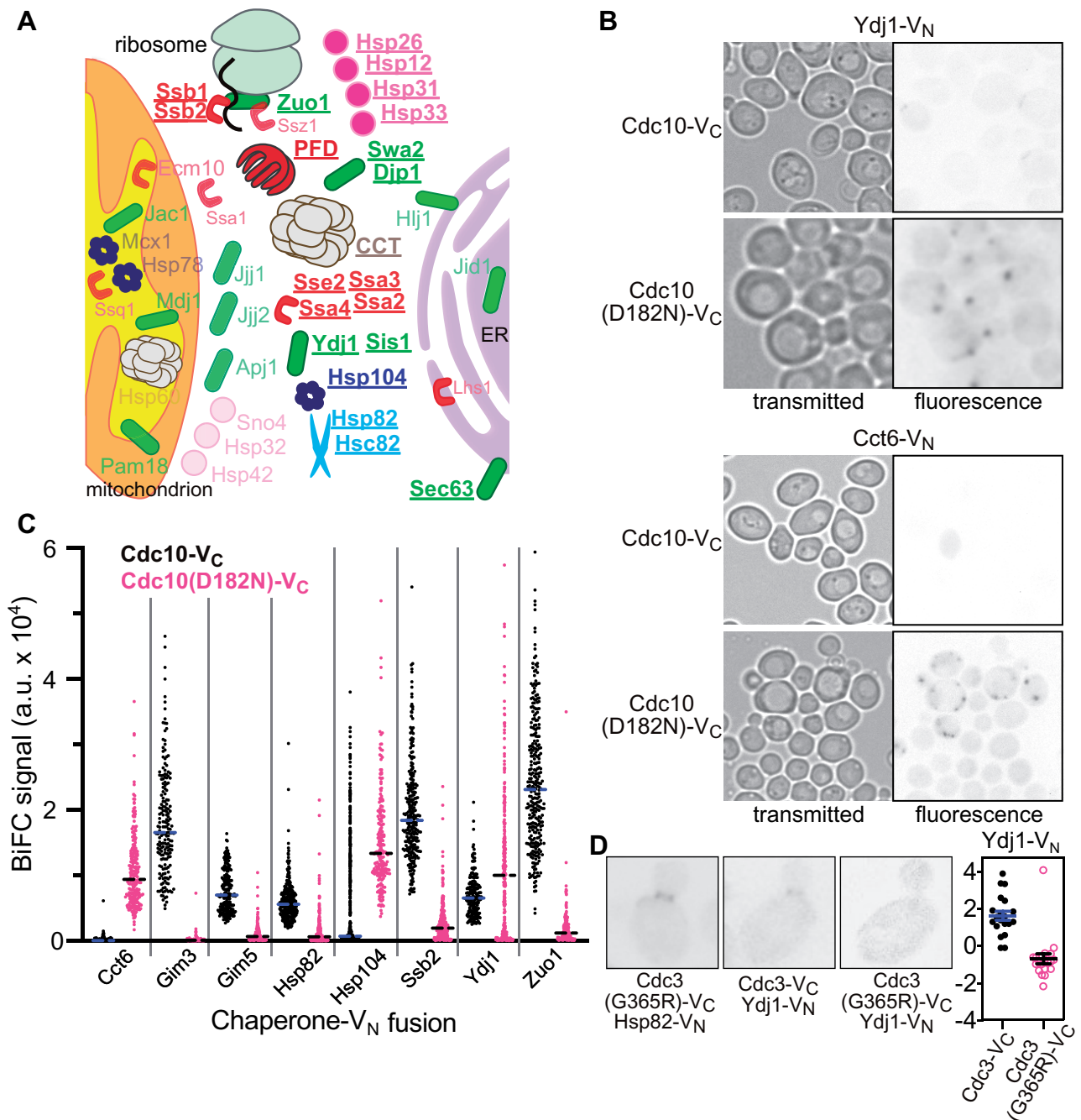
Figure 1 BiFC reveals septin–chaperone interactions in living cells. (A) Graphical summary of interactions between V_C-tagged septins and V_N-tagged cytosolic chaperones in diploid cells coexpressing untagged versions of all proteins. Chaperones that generated discrete fluorescence signal are in bold and underlined. See Table 1 for full dataset. Chaperones are color-coded by family and chaperones from the same family are drawn as the same shape. For the multisubunit chaperones PFD and CCT, if a single subunit interacted with any septin, then the entire complex is indicated as interacting with septins. (B) Micrographs showing discrete fluorescence signals in diploid cells coexpressing Cdc10-V_C or the D182N mutant derivative with Ydj1-V_N or Cct6-V_N. The fluorescence images were inverted to facilitate viewing. Red arrowheads point to bud neck signal. Strains were diploids made by mating YO1057 with H00385 or H00382. (C) Cellular BiFC signal away from bud necks was quantified for diploid cells coexpressing Cdc10-V_C or Cdc10(D182N)-V_C and the indicated V_N-tagged chaperones. The number of cells analyzed for each genotype ranged from 113 to 460. Strains were diploids made by mating YO1057 or H06530 with H00382, H00392, H00390, H00398, H00384, H00394, H00385, or H00396. (D) Representative images of diploid cells (strain M-1622 mated with H00398 or H00385) carrying *cdc3(G365R)* at one allele of *CDC3* and WT *CDC3* at the other, a V_N-tagged allele of the indicated chaperone at one allele of the chaperone gene locus and an untagged allele at the other, and a low-copy plasmid (G00521 or G00522) encoding Cdc3-V_C or Cdc3(G365R)-V_C. Plot at right shows quantification of bud neck fluorescence. Twenty cells were analyzed for each genotype.

Septin–chaperone BiFC

To measure bud neck BiFC fluorescence (Figure 1C) we used an existing macro (Weems and McMurray 2017) with FIJI software (Schindelin *et al.* 2012). To measure intracellular BiFC signal not focused on the bud neck, we used FIJI to adjust the brightness/ contrast on transmitted light images of fields of cells and then used the Threshold function to create a binary image with cell outlines. The "Fill Holes" process was used to fill cell outlines, and then this binary image was used as a mask to measure the integrated signal intensity and areas for the fluorescence image

of the same field of cells. To avoid non-cell particles, measurements were restricted to particles with areas between 500 and 2000 square pixels and circularity 0.5–1.0. Occasional cells (<1%) with extremely bright fluorescence were presumed to be dead and were excluded.

p53–chaperone BiFC

Haploid BY4742 cells carrying relevant plasmids described in figure legends were mated to V_N-fusion strains encoding a V_N-tagged chaperone . Diploids were inoculated in liquid synthetic medium with 1.9% raffinose and 0.1% galactose lacking leucine and uracil and imaged after growing to $OD_{600}\sim1$ at 30°. For each chaperone the series of WT p53, p53(V272M), and p53(R273H) were imaged in parallel. Micrographs were quantified for Venus and mKate2 signal ($n = 100$ cells for each genotype per chaperone) using FIJI software (Schindelin *et al.* 2012) and a macro that allowed selection and quantification of Venus and mKate2 signals from the same cell location (the cytosol, the nucleus, or both depending on the location of BiFC interactions). Relevant macros are available on GitHub (https://github.com/michael-mcmurray/Denney-et-al-G3-2021/).

p53–p53 BiFC

Haploid Y0134 cells carrying relevant plasmids described in figure legends were inoculated in liquid synthetic medium with 2% glucose lacking leucine and tryptophan and imaged after growing to $OD_{600}\sim0.5$ at 37°. Micrographs were quantified for nuclear Venus and mKate2 signal ($n = 100$ cells for each genotype) using FIJI software (Schindelin *et al.* 2012) and a macro that allowed selection and quantification of Venus and mKate2 signals from the same cell location. Cells were selected for quantification based on the presence of Venus signal, as not all cells with mKate2 signal had generated and matured Venus signal, but all cells with Venus signal had corresponding mKate2 signal.

p53 localization assays

For kinetics of p53 nuclear accumulation, haploid yJM3164 cells carrying relevant plasmids were inoculated from overnight liquid cultures grown at 24° in synthetic medium with 2% raffinose lacking tryptophan into fresh medium with 1.9% raffinose and 0.1% galactose and imaged every 30 min for 6 h at 24°, and finally again at 10 h. Micrographs were quantified for GFP and mKate2 signal ($n = 100$ cells for each genotype per timepoint) using FIJI software (Schindelin *et al.* 2012) and a macro that allowed selection and quantification of GFP and mKate2 signals from the nucleus. Note that GFP was used here only to verify the location of the nucleus and GFP quantities were not analyzed further.

For steady-state levels of p53 at different temperatures, haploid yJM3164 cells carrying relevant plasmids described in figure legends were inoculated in liquid synthetic medium lacking leucine and imaged after growing to $OD_{600}\sim0.5$ at 30° or 37°. Micrographs were quantified for GFP and mKate2 signal ($n = 100$ cells for each genotype per temperature) using FIJI software (Schindelin *et al.* 2012) and a macro that allowed selection and quantification of GFP and mKate2 signals from the nucleus. Note that GFP was used here only to verify the location of the nucleus and GFP quantities were not analyzed further.

For p53 localization with chaperone overexpression, diploid yJM3164 × yJM1838 cells carrying relevant plasmids described in figure legends were inoculated in liquid synthetic medium with 2% galactose and 2% raffinose but lacking leucine and tryptophan and imaged after growing to OD600~1 at 30°. Micrographs were quantified for GFP and mKate2 signal ($n = 100$ cells per

genotype) using FIJI software (Schindelin *et al.* 2012) and a macro that allowed selection and quantification of GFP and mKate2 signals from the nucleus and cytosol. Note that GFP was used here only to verify the location of the nucleus (and by exclusion, the cytosol) and GFP quantities were not analyzed further.

For p53 localization with Hsp90 inhibition, haploid yJM3164 cells carrying relevant plasmids described in figure legends were inoculated in liquid synthetic medium with 2% glucose lacking leucine and containing 5 μg/ml radicicol or equal volume DMSO and imaged after growing to $OD_{600}\sim0.5$ at 37°. Micrographs were quantified for nuclear GFP and mKate2 signal ($n = 100$ cells per genotype) using FIJI software (Schindelin *et al.* 2012) and a macro that allowed selection and quantification of GFP and mKate2 signals from the nucleus and cytosol. Note that GFP was used here only to verify the location of the nucleus (and by exclusion, the cytosol) and GFP quantities were not analyzed further.

Coimmunoprecipitation and immunoblotting

Twenty-five milliliter yeast cultures in liquid synthetic medium lacking leucine and tryptophan were grown to $OD_{600}\sim1$ at 30° and pelleted. Pellets were washed with Lysis Buffer (20 mM Tris-HCl pH 7.4, 150 mM NaCl, 1 mM EDTA, 0.5% Triton X-100, 1 mM DTT) plus protease inhibitors (Complete EDTA-free; 11 873 580 001, Roche) and frozen in liquid nitrogen. Pellets were resuspended in 300 μl ice-cold Lysis Buffer plus protease inhibitors and lysed using 100 μl glass beads and eight cycles of 30-s on/off vortexing at 4°. Lysates were clarified by centrifugation into new tubes. Clarified lysates were diluted 1:2.5 in Binding Buffer (10 mM Tris-HCl pH 7.4, 150 mM NaCl, 0.5 mM EDTA, 1 mM DTT) for a total volume of 700 μl "Input." 25 μl Chromotek GFP-nAb Magnetic Agarose beads (Chromotek, Germany) were washed three times with Binding Buffer and combined with 700 μl diluted lysate. Beads were incubated while tumbling end-over-end for 1 h at 4°. "Unbound" fraction was removed and beads washed once with Binding Buffer and twice with Wash Buffer (10 mM Tris-HCl pH 7.4, 500 mM NaCl, 0.5 mM EDTA, 1 mM DTT). Beads were resuspended and gently pipetted in 50 μl 2× SDS-PAGE sample buffer plus 5% β-mercaptoethanol and heated at 95° for 5 min to generate the "Bound" fraction. Following SDS-PAGE, proteins were electrophoretically transferred to PVDF and exposed to mouse anti-p53 (RRID: AB_10986581) and rabbit anti-Pgk1 primary antibodies. Infrared-labeled antimouse (680 nm, RRID: AB_10854088) and antirabbit (800 nm, RRID: AB_10697505) secondary antibodies were applied before scanning on a Licor Odyssey device. Input represents 7% of the amount of total protein used for the amount of immunoprecipitated material loaded on the gel.

For all other immunoblots, cultures were grown to mid-log phase and pellets were washed with 10% trichloroacetic acid (TCA) and frozen in liquid nitrogen, then placed at −70°C. Cell pellets were thawed in 150 μl of 1.85 M NaOH and 7.4% β-mercaptoethanol. 150 μl of 50% TCA was added before incubation on ice for 10 min. Precipitated proteins were pelleted at 4°C at maximum speed for 10 min, washed twice with cold acetone (1 ml each time), and resuspended in 80 μl of 0.1 M Tris base, 5% SDS. After addition of SDS-PAGE sample buffer, the samples were boiled for 5 min before resolution by SDS-PAGE. Membrane processing was the same as described above and also utilized, where indicated, mouse anti-6xHis antibodies (UBPBio no. Y1011). Ponceau solution (0.5% w/v, 1% acetic acid), where indicated, was applied for 30 min, then washed with water and the membrane allowed to dry before imaging.
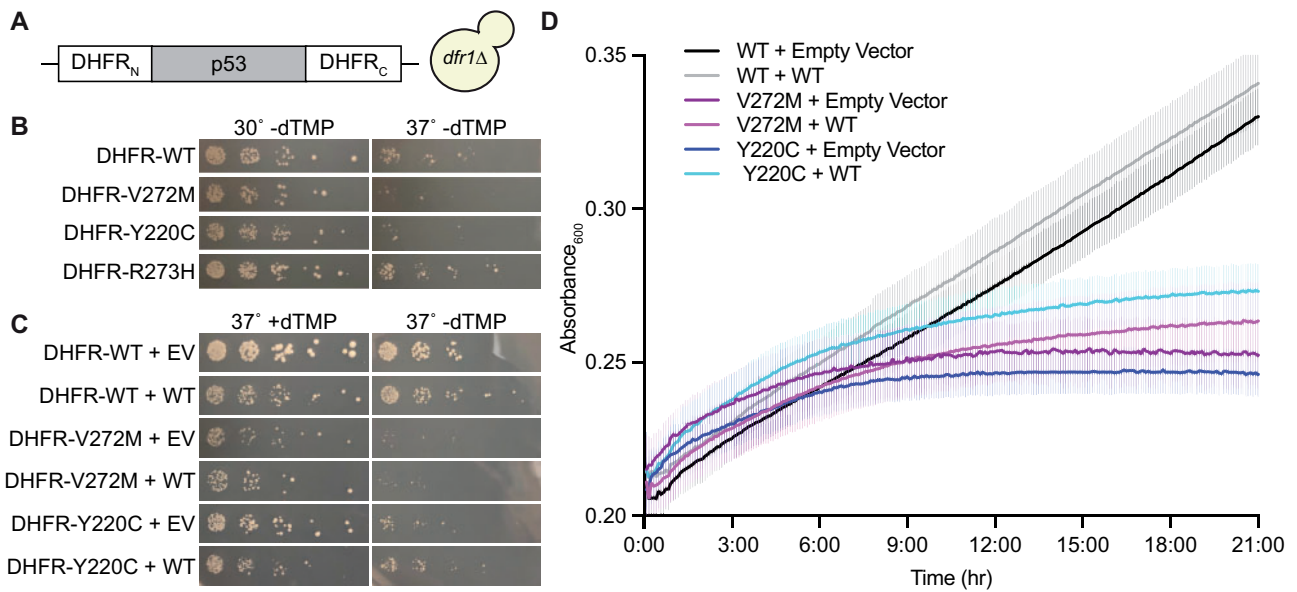
Figure 2 Coexpression of WT p53 fails to rescue the folding defects of the p53(V272M) mutant at high temperature. (A) Illustration of split-DHFR p53 construct. TH5 cells are *dfr1Δ* and proliferate only when exogenous dTMP is present or p53 folds well enough to reconstitute active DHFR. (B) Colony growth at 30° and 37° by fivefold serially diluted TH5 cells carrying plasmids encoding the indicated p53 split DHFR alleles spotted on solid synthetic medium selective for the plasmids and lacking dTMP. Plasmids were G00598, "DHFR-WT"; G00604, "DHFR-V272M"; G00599, "DHFR-Y220C"; G00605, "DHFR-R273H." (C) As in (B), but with cells also carrying a plasmid encoding WT p53 (pLS76) or an empty vector ("EV," pRS415) on solid medium selective for the plasmids and either containing "+" or lacking "−" dTMP at 37°. (D) As in (C) except cells were grown in liquid medium without dTMP at 37° in a flat-bottom 96-well plate. Optical density at 600 nm was recorded at 5-min intervals over 21 h for 6 replicate cultures per genotype and plotted as mean (thick line) and upper and lower bounds of the 95% C.I. (thin lines).

Choice of sample sizes and statistical analysis

Sample sizes (number of cells) for fluorescence microscopy were chosen based on our ability to detect changes in subcellular localization in our previous studies (Johnson *et al.* 2015, 2020; Weems and McMurray 2017). Analysis of effect sizes and generation of effect size plots were performed using DABEST (data analysis with bootstrap-coupled estimation; Ho *et al.* 2019) via the online server at http://www.estimationstats.com.

Results

BiFC as an approach to trap otherwise transient chaperone–client interactions

In principle, the chaperone–septin interactions we found using biochemical approaches (Johnson *et al.* 2015) could have occurred following cell lysis. To visualize chaperone–septin interactions in intact, living cells, we used a BiFC approach, also called split-YFP. Reconstitution of Venus, an YFP derivative, occurs when two nonfluorescent Venus fragments, V_N and V_C, are brought in close proximity. Fusion of V_N and V_C to two proteins that directly interact *in vivo* is typically sufficient to drive Venus reconstitution. Although the interactions driving its folding and chromophore maturation are non-covalent, Venus reconstitution is effectively irreversible *in vivo*. Consequently, BiFC can be used to generate a stable fluorescent signal from otherwise transient interactions in which the untagged proteins would normally dissociate (Hu *et al.* 2002). Chromophore maturation requires considerable additional time after Venus folding, up to 50 min (Kerppola 2008); hence, signal intensity over time also depends on the half-life of the "crosslinked" fusion proteins. Since chaperone–client interactions are transient by definition, BiFC is ideally suited for detecting such interactions *in vivo*.

Venus fragments are misfolded proteins that could act as "chaperone bait" independent of the protein to which they are fused. Indeed, multiple V_C-tagged chaperones (Hsp12, Hsc82, Hsp82, Hsp104, Ssa1, Ssb1, Ssb2, Sec63, Sis1, and Zuo1) are known to generate BiFC signals when coexpressed with "free" V_N (Kim *et al.* 2019). We reasoned that the smaller size of V_C (∼120 residues, ∼13.5 kDa) compared with V_N (∼190 residues, ∼21 kDa) might make it less prone to nonspecific chaperone interactions. We therefore mated haploid yeast cells expressing V_C-tagged septins with haploid cells expressing V_N-tagged chaperones and after culturing the resulting diploid cells at room temperature (∼22°) we examined them by epifluorescence microscopy. We tested 48 V_N-tagged chaperones with all five V_C-tagged mitotic septins (Cdc3, Cdc10, Cdc11, Cdc12, and Shs1). As shown in Figure 1 and summarized in Figure 1A and Table 1, we observed discrete fluorescence signals for multiple cytosolic chaperones. In most cases these signals were found in either of two general subcellular locations. Although some diffuse BiFC signal was also faintly visible (see below), we focused first on the much more obvious discrete signals.

The first location of BiFC signal, observed with numerous chaperones, resembled the typical localization observed for native septins: rings at the cortex (Figure 1B, Supplementary Figure S1A, and Table 1). Cortical rings were seen either exclusively at the bud neck, where septin rings are normally found, or faintly at bud necks and more intensely at locations reminiscent of bud-site-selection landmark proteins that persist at previous sites of budding (Supplementary Figure S1A). In unstressed cells, most fluorescently tagged cytosolic chaperones are found distributed diffusely throughout the cytosol (Huh *et al.* 2003). We think it is most likely that for the chaperones generating cortical ring fluorescence, BiFC events arose from transient septin–chaperone
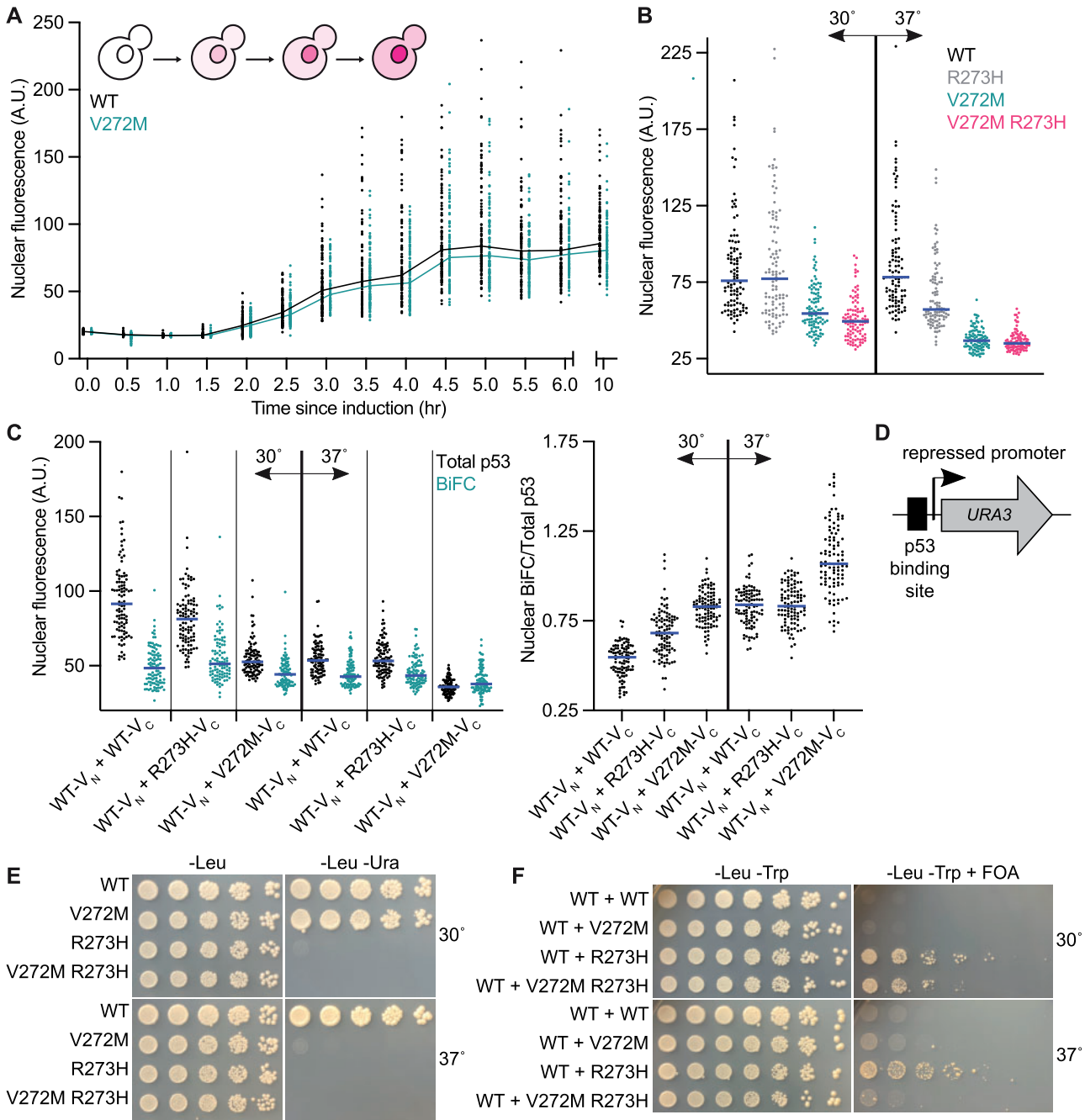
Figure 3 Effects of the V272M and R273H mutations on p53 nuclear localization, oligomerization, and function. (A) Nuclear mKate2 fluorescence in yJM3164 cells carrying a plasmid encoding *GAL1/10*-driven p53-mKate2-V$_C$ (H3.29) or p53(V272M)-mKate2-V$_C$ (pMAM67). Cells were imaged at 30-min intervals following induction with galactose at 24°. Lines connect median values; for clarity of viewing, the positions on the x axis were slightly "nudged" so that the two samples do not overlap on the plot. The schematic illustrates accumulation of nuclear and cytosolic p53 over time. (B) Steady-state nuclear mKate2 fluorescence of yJM3164 cells carrying plasmids encoding the indicated alleles of p53-mKate2-Venus and grown to mid-log phase at 30° or 37°. Blue lines denote median values. Vertical line separates 30° from 37°. Plasmids were pMAM85, "WT"; pMAM87, "R273H"; pMAM86, "V272M"; pMAM104, "V272M R273H." (C) As in (B) but with cells of strain Y0134 coexpressing two p53 alleles fused to mKate2 and the indicated Venus fragments. Venus fluorescence here indicates physical interaction (BiFC). Left plot, total p53 (mKate2) and BiFC (Venus) nuclear fluorescence. Right plot, BiFC (Venus) nuclear signal normalized to total p53 (mKate2) nuclear signal. Blue lines denote median values. Vertical lines separate genotypes. Bold vertical lines separate 30° from 37°. Plasmids were pMAM98, "WT-V$_N$"; pMAM82, "WT-V$_C$"; pMAM84, "R273H-V$_C$"; pMAM83, "V272M-V$_C$." (D) Schematic of p53 transcriptional reporter strains RBy33 and RBy159. Binding of properly folded p53 to a repressed promoter activates transcription of the *URA3* gene product, leading to colony growth on medium lacking uracil, or inhibition of growth on medium containing FOA. (E) Colony growth at 30° and 37° by RBy33 cells carrying plasmids encoding the indicated alleles of p53 on medium selective for the plasmids "-Leu" or selective for the plasmid and p53 reporter activity "-Leu –Ura." Plasmids were pLS76, "WT"; pMAM69, "V272M"; pMAM79, "R273H"; pMAM77, "V272M R273H." (F) Colony growth at 30° and 37° by diploid cells with the *URA3* reporter of p53 activity carrying plasmids encoding the indicated alleles of p53, together with WT p53 plasmid, on solid medium selective for the plasmids "-Leu -Trp" or selective for the plasmids and counter-selective for p53 reporter activity "-Leu -Trp + FOA." Plasmids were pMAM78 and pLS76, "WT"; pMAM69, "V272M"; pMAM79, "R273H"; pMAM77, "V272M R273H." Strains were diploids made by mating RBy33 cells carrying pLS76, pMAM69, pMAM79, or pMAM77 with RBy159 cells carrying pMAM78.
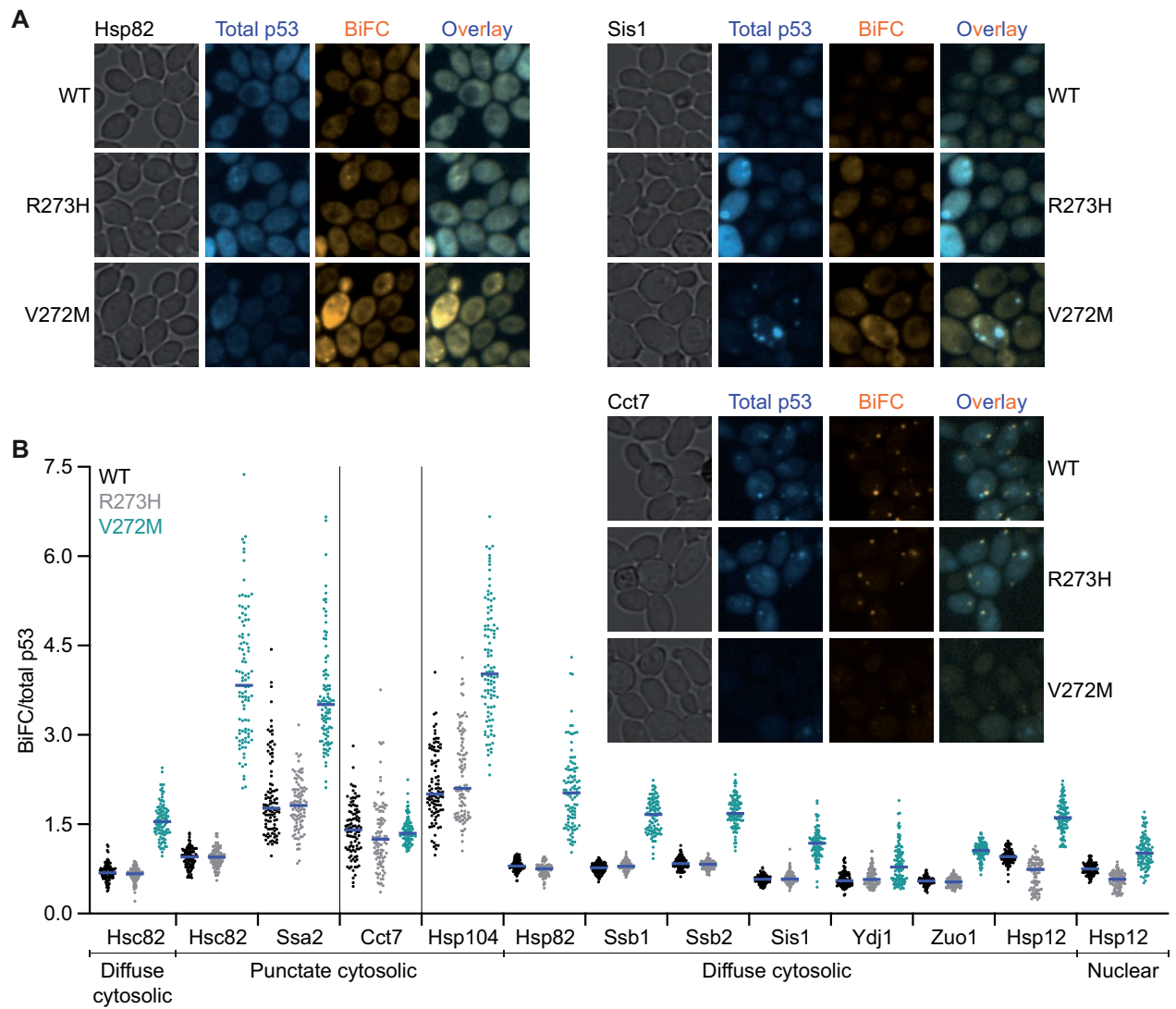
Figure 4 Cytosolic chaperone-p53 interactions in living cells. (A) Representative micrographs of p53–chaperone BiFC interactions in cells cultured at 30° and expressing Hsp82-V_N, Sis1-V_N, or Cct7-V_N and carrying plasmids encoding the indicated p53-mKate2-V_C alleles. Total p53 (mKate2) fluorescence images were false-colored blue and BiFC (Venus) fluorescence images were false-colored orange. Prior to overlay, brightness and contrast were adjusted equivalently for each set of images. Plasmids were pMAM110, "WT"; pMAM112, "R273H"; pMAM111, "V272M." Strains were diploids made by mating BY4742 cells carrying the plasmids with H00398, H06680, or H00383. (B) BiFC (Venus) signal normalized to total p53 (mKate2) signal in cells cultured at 30° carrying plasmids encoding the indicated p53-mKate2-V_C alleles together with the indicated V_N-tagged chaperone. Blue lines denote median values. Vertical lines group the samples imaged with the same settings (LED intensity and exposure time). The subcellular location where the BiFC interaction was quantified is indicated below. Plasmids were pMAM110, "WT"; pMAM112, "R273H"; pMAM111, "V272M." Strains were diploids made by mating BY4742 cells carrying the plasmids with H00399, "Hsc82"; H00388, "Ssa2"; H00383, "Cct7"; H00384, "Hsp104"; H00398, "Hsp82"; H00395, "Ssb1"; H00394, "Ssb2"; H06680, "Sis1"; H00385, "Ydj1"; H00396, "Zuo1"; or H06684, "Hsp12."

interactions in the cytosol. The tagged chaperone was then forced to follow the tagged septin on its subsequent cortical journeys. We interpret BiFC signal at bud necks as representing "crosslinked" septin-V_C-chaperone-V_N complexes in which the septin incorporated into septin hetero-oligomers and then into septin filaments, with the tagged chaperone becoming tethered to the septin ring. Due to the delay between initial interaction and fluorophore maturation, by microscopy we see only "old" septin–chaperone "crosslinked" complexes that may have already been through multiple rounds of filament polymerization and depolymerization. The appearance of bright cortical rings at sites of prior budding for some chaperones may indicate that those specific septin-chaperone BiFC associations perturbed the disassembly of "old" septin rings that normally follows each cell division,

such that new rings are dimmer because they preferentially incorporate "new" or untagged septins.

The second type of discrete BiFC signal was unique to interactions between WT septins and subunits of the cytosolic chaperonin called CCT (chaperonin containing tailless complex polypeptide 1). Coexpression of Cct7-V_N with Cdc3-V_C Cdc10-V_C, or Cdc12-V_C generated discrete puncta in a subpopulation of cells (Supplementary Figure S1A and Table 1). We engineered haploid strains carrying Cct7-V_N and Cdc3-V_C and confirmed that the punctate BiFC signal was not unique to diploid cells (Supplementary Figure S1A). That these haploids were viable and of normal morphology indicates that the septin–Cct7 BiFC interaction did not perturb essential CCT functions, and that only some of the Cdc3-V_C molecules underwent BiFC events,
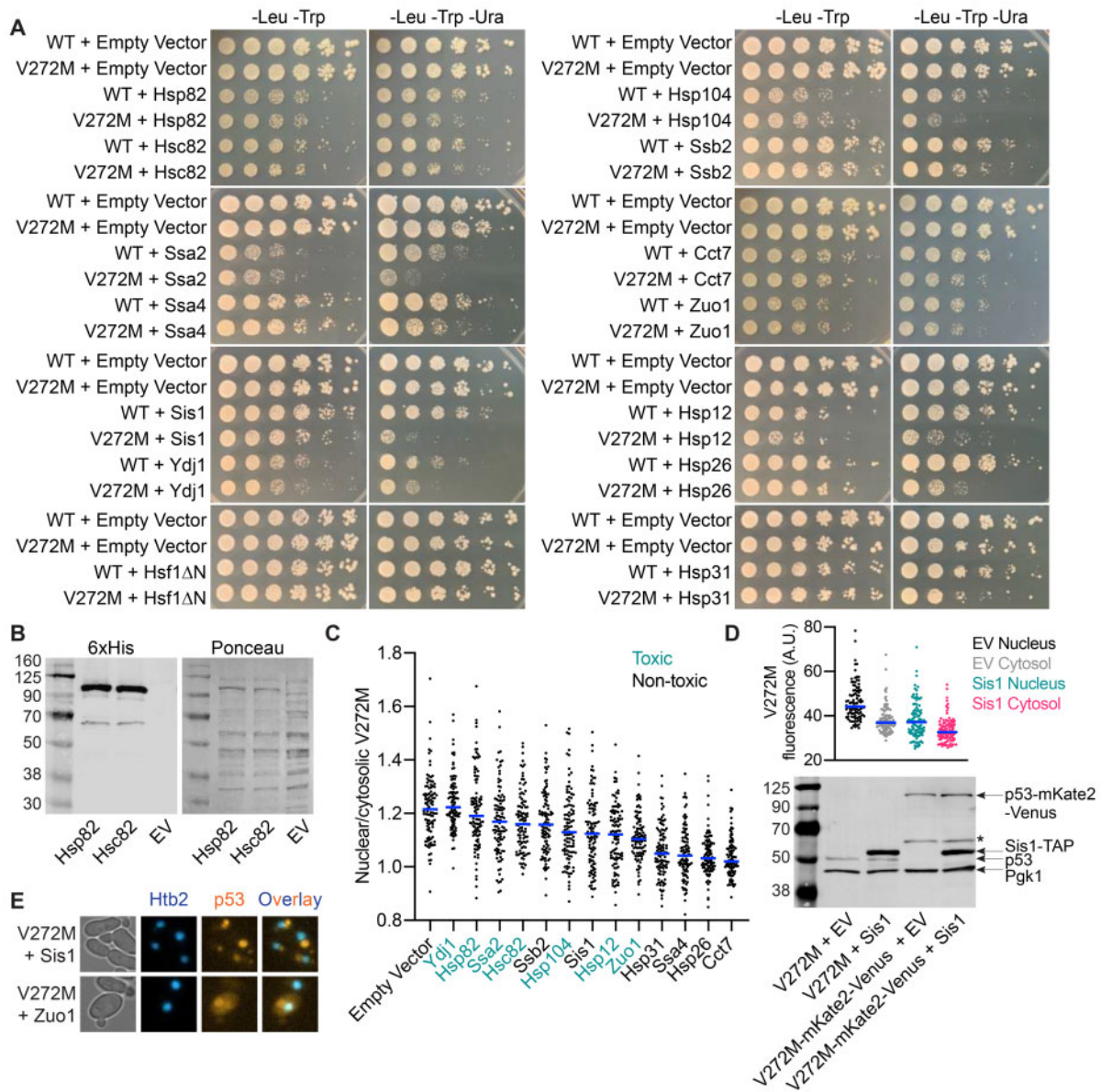
Figure 5 Overexpression of specific chaperones inhibits p53(V272M) function. (A) Colony growth at 30° of fivefold serially diluted diploid cells with the *URA3* reporter of p53 activity carrying plasmids encoding the indicated alleles of p53, together with the indicated *GAL1/10*-driven chaperone plasmid or an empty vector, on solid galactose medium selective for the plasmids "-Leu -Trp" or selective for the plasmids and p53 reporter activity "-Leu -Trp –Ura." Plasmids were pLS76, "WT"; pMAM69, "V272M"; pRS424 and pRS314, "Empty Vector"; G00630, "Hsp82"; G00799, "Hsc82"; G00633, "Ssa2"; G00789, "Ssa4"; G00632, "Sis1"; G00353, "Ydj1"; G00061, "Hsf1ΔN"; G00631, "Hsp104"; G00634, "Ssb2"; G00620, "Cct7"; G00635, "Zuo1"; G00627, "Hsp12"; G00628, "Hsp26"; G00629, "Hsp31." Strains were diploids made by mating RBy33 cells carrying pLS76 or pMAM69 with RBy159 cells carrying the *GAL1/10*-driven chaperone plasmid or empty vector. (B) SDS-PAGE and immunoblot analysis of total protein extracts from diploid cells carrying a plasmid encoding p53(V272M) (pMAM69) together with a *GAL1/10*-driven Hsp82 plasmid (G00630), a *GAL1/10*-driven Hsc82 plasmid (G00799), or an empty vector (pRS424, "EV") grown to mid-log phase at 30° in medium with galactose to induce overexpression. The membrane was first probed for hexahistidine-tagged Hsp82 and Hsc82 and subsequently stained with Ponceau. (C) Ratio of nuclear to cytosolic mKate2 signal in diploid cells carrying a plasmid encoding p53(V272M)-mKate2-Venus together with the indicated *GAL1/10*-driven chaperone plasmid or an empty vector. Cells were grown to mid-log phase at 30° with galactose to overexpress chaperones prior to imaging. "Toxic" denotes chaperones whose overexpression renders p53 inhibitory to colony growth independent of p53 function. Blue lines denote median values. Plasmids were pMAM86, "p53(V272M)"; pRS424, "Empty Vector"; G00353, "Ydj1"; G00630, "Hsp82"; G00633, "Ssa2"; G00799, "Hsc82"; G00634, "Ssb2"; G00631, "Hsp104"; G00632, "Sis1"; G00627, "Hsp12"; G00635, "Zuo1"; G00629, "Hsp31"; G00789, "Ssa4"; G00628, "Hsp26"; G00620, "Cct7." Strains were diploids made by mating yJM3164 cells carrying pMAM86 with yJM1838 cells carrying the indicated *GAL1/10*-driven chaperone plasmid or empty vector. (D) Top, nuclear and cytosolic mKate2 fluorescence in diploid cells carrying a plasmid encoding p53(V272M)-mKate2-Venus (pMAM86) and an empty vector ("EV," pRS424) or a plasmid encoding tandem affinity purification-(TAP-)tagged Sis1 (G00632). Cells were grown to mid-log phase at 30° with galactose to overexpress Sis1 prior to imaging. A single outlier (Y = 115) was omitted from the EV Nucleus dataset to facilitate viewing on the Y-axis. Blue lines denote median values. Strains were diploids made by mating yJM3164 cells carrying pMAM86 to yJM1838 cells carrying G00632 or pRS424. Bottom, as in (B) but with diploid cells carrying plasmids encoding the indicated alleles of p53 together with the Sis1-TAP plasmid or an empty vector, as in (A) or the plot above, and probed for p53, the cytosolic protein Pgk1, and hexahistidine-tagged Sis1-TAP. Asterisk, proteolytic degradation products derived from p53-mKate2-Venus. (E) Representative micrographs of vacuolar mKate2 signal in diploid cells expressing p53(V272M)-mKate2-Venus (pMAM86) and *GAL1/10*-driven Sis1 (G00632) or *GAL1/10*-driven Zuo1 (G00616), prepared as in (C). Nucleus (Htb2-mNeon) fluorescence images were false-colored blue and p53 (mKate2) fluorescence images were false-colored orange. Prior to overlay, brightness, and contrast were adjusted equivalently for each set of images. Strain was a diploid made by mating yJM3164 cells carrying pMAM86 to yJM1838 cells carrying G00632 or G00616.

otherwise no Cdc3-V_C would have been available to perform septin functions at the bud neck. In stressed cells, other chaperones (*e.g.*, Hsp104) localize to punctate structures together with misfolded proteins, such as the IPOD (insoluble protein deposit) and/or JUNQ (juxtanuclear quality control; Kaganovich *et al.* 2008), but the Cct7–septin BiFC puncta did not colocalize with Act1(E364K)-mCherry, a misfolded form of actin that marks these compartments (Supplementary Figure S1B). CCT subunit C termini project into the center of the chamber (Llorca *et al.* 1999), hence Cct7-V_N–septin-V_C interactions likely occur when septins are inside, as opposed to interacting with the chamber surface. Although each individual CCT subunit is relatively small, the cage-shaped holoenzyme is large (~1 MDa). We interpret the appearance of puncta as evidence that following BiFC association the tagged septin remains tethered to the inside of the chamber, and is unavailable for incorporation into septin-based structures. CCT assemblies with septins tethered via BiFC may be unable to fold other proteins, but why they would accumulate abnormally in a single intracellular location is a mystery. We cannot exclude the alternative possibility that Cct7-V_N interacts with septins prior to assembling into a 16-mer; "free" Cct7-V_N could interact with septins in a way that, when tethered to the septin via the BiFC connection, perturbs septin folding and drives aggregation in a way that does not involve the CCT holoenzyme. The apparent ability of Cdc3-V_C to frequently "escape" Cct7-V_N interaction could

mean that some Cdc3 never interacts with CCT that some Cdc3–CCT interactions are too transient for BiFC, and/or that Cdc3–CCT interactions do not always involve the Cct7 subunit.

Individual CCT subunits make client-specific contacts. For example, actin directly contacts only five CCT subunits (Balchin *et al.* 2018). When CCT is dissociated into individual subunits, Shs1 copurifies with Cct6 but not with Cct3 (Dekker *et al.* 2008), suggestive of some specificity in CCT–septin interactions. Indeed, Cct7-V_N interacted with Cdc3-V_C, Cdc10-V_C, and Cdc12-V_C, but did not exhibit a BiFC signal with Shs1-V_C or its paralog Cdc11-V_C (Table 1). We did not detect punctate septin BiFC signal with V_N-tagged Cct2, Cct3, Cct4, or Cct6 in cells cultured at room temperature; Cct1/Tcp1, Cct5, and Cct8 are not in the V_N tag collection and thus were not tested. Another multisubunit chaperone complex, prefoldin, also displayed subunit-specific BiFC interactions with septins (Table 1).

Temperature affects both protein folding and the expression of most chaperones. To ask if our BiFC system was able to capture such changes, we repeated our analysis in cells cultured at 37°. The spectrum of chaperone interactions at this temperature was mostly unchanged, with a few notable exceptions. At 37° Cct2, Cct3, and Cct6 showed detectable signal, as discrete puncta similar to what we saw for Cct7 at room temperature (Table 1 and data not shown). Other septin–chaperone BiFC signals
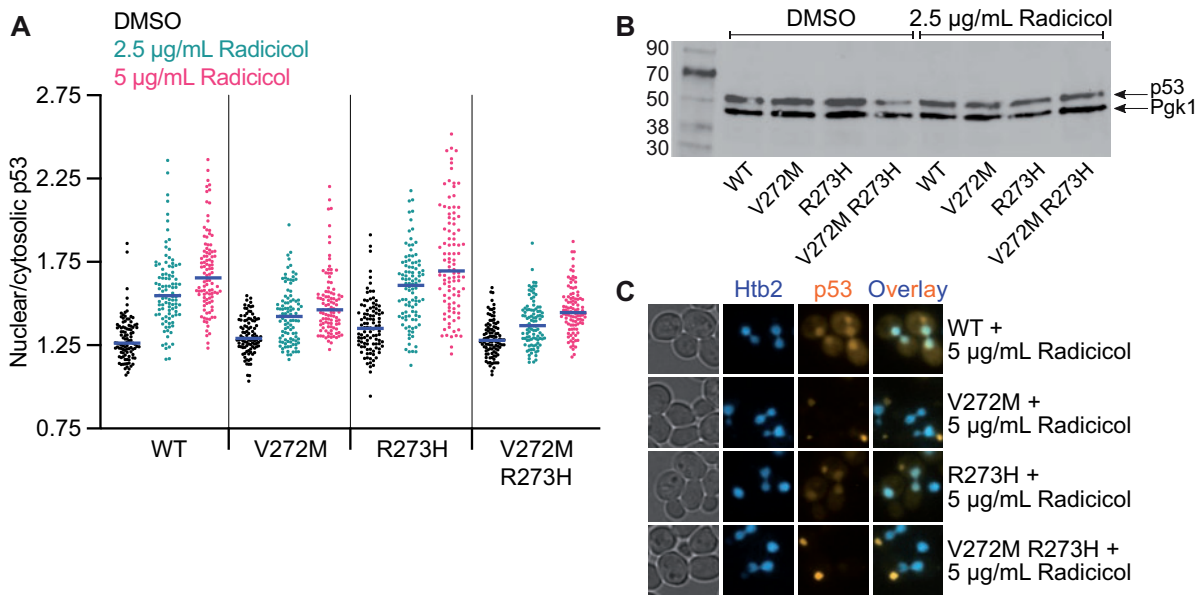

Figure 6 Chaperone inhibition liberates p53 from cytosolic compartmentalization. (A) Ratio of nuclear to cytosolic mKate2 signal in yJM3164 cells carrying plasmids encoding the indicated alleles of p53-mKate2-Venus. Cells were grown to mid-log phase at 37° with 2.5 μg/ml radicicol or equivalent volume of DMSO prior to imaging. Blue lines denote median values. Vertical lines separate genotypes. Plasmids were pMAM85, "WT"; pMAM86, "V272M"; pMAM87, "R273H"; pMAM104, "V272M R273H." (B) RBy33 cells carrying plasmids encoding the indicated alleles of p53 were grown to mid-log phase at 30° and lysed. Proteins were separated by SDS-PAGE. After electrophoretic transfer, the membrane was probed for p53 and the cytosolic protein Pgk1. Plasmids were pLS76, "WT"; pMAM69, "V272M"; pMAM79, "R273H"; pMAM77, "V272M R273H." (C) Representative micrographs of vacuolar mKate2 signal in yJM3164 cells carrying plasmids encoding the indicated alleles of p53-mKate2-Venus and treated with 5 μg/ml radicicol, prepared as in (A). Nucleus (Htb2-mNeon) fluorescence images were false-colored blue and p53 (mKate2) fluorescence images were false-colored orange. Prior to overlay, brightness, and contrast were adjusted equivalently for each set of images. Plasmids were pMAM85, "WT"; pMAM86, "V272M"; pMAM87, "R273H"; pMAM104, "V272M R273H."

Table 1. Septin–chaperone interactions generating discrete BiFC signals

Chaperone (family)[a]	Major cellular compartment (minor)[b]	Room temperature Septin BiFC interactions (variable)[c]	37° Septin BiFC interactions (variable)[c]	Published evidence[d]
Ssa1 (Hsp70)	Cytosol (Nucleus)	—	—	
Ssa2 (Hsp70)	Cytosol (Mitochondria)	Cdc3*, Cdc10, Cdc11, Cdc12, and Shs1	Cdc3*, Cdc10, Cdc11, Cdc12, and Shs1	
Ssa3 (Hsp70)	Cytosol	Cdc3, Cdc10, Cdc11, Cdc12, and Shs1	(Cdc10), (Cdc12), and(Shs1)	
Ssa4 (Hsp70)	Cytosol (Nucleus)	Cdc3, Cdc10, Cdc11, Cdc12, and Shs1	Cdc10 and Cdc12	
Ssb1 (Hsp70)	Cytosol	Cdc3, Cdc10, Cdc11, Cdc12, and Shs1	Cdc3, Cdc10, Cdc11, Cdc12, and Shs1	Cdc3 (P) (Stein *et al.* 2019), Cdc10 (P) (Stein *et al.* 2019), and Cdc11 (P) (Stein *et al.* 2019)[e]
Ssb2 (Hsp70)	Cytosol	Cdc3, Cdc10, Cdc11, Cdc12, and Shs1	Cdc3, Cdc10, Cdc11, Cdc12, and Shs1	Cdc3 (P) (Stein *et al.* 2019), Cdc10 (P) (Stein *et al.* 2019), and Cdc11 (P) (Stein *et al.* 2019)[e]
Sse2 (Hsp70)	Cytosol	Cdc3, Cdc10, Cdc11, Cdc12, and (Shs1)	—	
Ssz1 (Hsp70)	Cytosol	—	Not tested	
Apj1 (Hsp40)	Cytosol (Nucleus, Mitochondria)	—	Not tested	
Djp1 (Hsp40)	Cytosol	Cdc3, Cdc10, (Cdc11), Cdc12, and (Shs1)	Not tested	
Jjj1 (Hsp40)	Cytosol (Nucleus, Mitochondria)	—	Not tested	
Jjj2 (Hsp40)	Cytosol (Nucleus)	—	Not tested	
Sis1 (Hsp40)	Cytosol (Nucleus)	Cdc3, Cdc10, Cdc11, Cdc12, and Shs1	Not tested	
Swa2 (Hsp40)	Cytosol (ER Membrane)	Cdc3, Cdc10, and (Cdc12)	Not tested	
Ydj1 (Hsp40)	Cytosol (ER Membrane)	(Cdc3), (Cdc10), Cdc11, Cdc12, and (Shs1)	(Cdc11) and (Cdc12)	Cdc10 (F) (Costanzo *et al.* 2010)
Zuo1 (Hsp40)	Cytosol (Nucleus)	Cdc3, Cdc10, Cdc11, Cdc12, and Shs1	Cdc3, Cdc10, Cdc11, Cdc12, and (Shs1)	
Hsp12 (small)	Cytosol (Nucleus)	Cdc3, Cdc10, Cdc11, Cdc12, and Shs1	Not tested	Cdc3 (F) (Costanzo *et al.* 2010)
Hsp26 (small)	Cytosol (Nucleus)	Cdc3*, Cdc10, Cdc11, Cdc12*, and Shs1	Not tested	
Hsp31 (small)	Cytosol	(Cdc3), Cdc10, Cdc11, Cdc12, and Shs1	(Cdc3), Cdc10, Cdc11, and (Cdc12)	Cdc3 (P) (Krogan *et al.* 2006)
Hsp32 (small)	Cytosol	—	Not tested	
Hsp33 (small)	Cytosol	(Cdc3) and (Cdc10)	Not tested	
Hsp42 (small)	Cytosol	—	Not tested	
Sno4 (small)	Cytosol	—	Not tested	
Hsp82 (Hsp90)	Cytosol (Mitochondria)	Cdc3*, Cdc10*, Cdc11*, Cdc12*, and Shs1*	Cdc3*, Cdc10*, Cdc11*, and Cdc12*	Cdc12 (P) (Millson *et al.* 2005), Shs1 (F) (Zhao *et al.* 2005)
Hsc82 (Hsp90)	Cytosol	Cdc3*, Cdc10*, Cdc11*, Cdc12*, and Shs1*	Cdc3*, Cdc10*, Cdc11*, Cdc12*, Shs1*	
Hsp104 (AAA+)	Cytosol (Nucleus)	Cdc3*, Cdc10*, Cdc11*, Cdc12*, and Shs1*	Cdc3*, Cdc10*, Cdc11*, Cdc12*, and (Shs1*)	Cdc11 (F) (Magtanong *et al.* 2011) and Cdc12 (F) (Schirmer *et al.* 2004)
CCT/TRiC (Type II chaperonin):	Cytosol	(Cdc3•), (Cdc10•), and (Cdc12•)	(Cdc10•), (Cdc11•), and (Cdc12•)	Cdc3 (P) (Stein *et al.* 2019), Cdc10 (P) (Stein *et al.* 2019; Yam *et al.* 2008), and Cdc11 (P) (Stein *et al.* 2019)
Cct2		—	(Cdc11•)	
Cct3		—	(Cdc10•) and (Cdc12•)	Cdc3 (P) (Dekker *et al.* 2008), Cdc10 (P) (Dekker *et al.* 2008), Cdc11 (P) (Dekker *et al.* 2008), Cdc12 (P) (Dekker *et al.* 2008), andShs1 (P) (Dekker *et al.* 2008)
Cct4		—	—	
Cct6		—	(Cdc10•)	Cdc3 (P) (Dekker *et al.* 2008), Cdc10 (P) (Dekker *et al.* 2008), Cdc12 (P) (Dekker *et al.* 2008), Shs1 (P) (Dekker *et al.* 2008)

(continued)

Table 1. (continued)

Chaperone (family)[a]	Major cellular compartment (minor)[b]	Room temperature Septin BiFC interactions (variable)[c]	37° Septin BiFC interactions (variable)[c]	Published evidence[d]
Cct7		(Cdc3•), (Cdc10•), and (Cdc12•)	(Cdc10•), (Cdc11•), and (Cdc12•)	
Prefoldin/GimC complex:	Cytosol	Cdc3, Cdc10, Cdc11, Cdc12, and Shs1	(Cdc10)	
Gim3		Cdc3, Cdc10, Cdc11, Cdc12, and Shs1	—	Cdc3 (F) (Costanzo et al. 2010)
Gim4		–	(Cdc10)	Cdc3 (P) (Wang et al. 2012)
Gim5		Cdc10, (Cdc11), and (Cdc12)	—	Cdc3 (P) (Wang et al. 2012)
Pfd1		(Cdc10) and (Cdc12)	—	
Yke2		(Cdc3), (Cdc10), and (Cdc12)	—	Cdc10 (F) (Collins et al. 2007)
Lhs1 (Hsp70)	ER lumen	—	—	
Hlj1 (Hsp40)	ER membrane	—	Not tested	
Sec63 (Hsp40)	ER membrane	Cdc3, Cdc10, Cdc11, Cdc12, and Shs1	Not tested	
Ecm10 (Hsp70)	Mitochondria	—	Not tested	
Ssq1 (Hsp70)	Mitochondria	—	Not tested	
Jac1 (Hsp40)	Mitochondria	—	Not tested	
Jid1 (Hsp40)	Mitochondria	—	Not tested	
Mdj1 (Hsp40)	Mitochondria	—	Not tested	
Hsp78 (AAA+)	Mitochondria	—	Not tested	Cdc3 (P) (Wang et al. 2012)
Mcx1 (AAA+)	Mitochondria	—	—	
Hsp60 (Type I chaperonin)	Mitochondria	—	Not tested	
Pam18 (Hsp40)	Inner mitochondrial membrane	—	Cdc3	Cdc12 (F) (Davierwala et al. 2005)

[a] For multisubunit complexes, cumulative interactions are listed in the same row, and individual tested subunits are listed below.
[b] Our interpretation of the literature regarding the major subcellular localization for the chaperone in question, with minor localizations given in parenthesis.
[c] "—," no discrete signal. *, fluorescence signal appeared as multiple cortical rings; •, punctate signal. Interactions generating fluorescence signal in only a subset of cells are indicated in parenthesis.
[d] (F), physical; (G), functional. Where the interaction could not be attributed to a specific subunit within a multisubunit chaperone, the septin interactor is listed on the same row as the multisubunit chaperone.
[e] The published experiment used a combination of anti-Ssb1 and -Ssb2 antibodies (Stein et al. 2019).

decreased at 37°. Septin interactions with prefoldin subunits almost completely disappeared at 37° (Table 1). Interactions between some septins (*e.g.*, Cdc10) and the Hsp40 Ydj1 were no longer detectable, and interactions with several cytosolic Hsp70-family chaperones were notably reduced (Table 1). Since many other chaperone interactions, including Hsp70s, were unchanged, an intrinsic reduction in the efficiency of Venus BiFC at 37° cannot explain the loss of specific chaperone signals. Instead, we attribute these changes to effects of temperature on septin folding—exposing different chaperone-interacting sequences—and/or chaperone expression levels.

Unique interactions between cytosolic chaperones and mutant septins that are kinetically delayed in their folding

Having established that WT septins associate with cytosolic chaperones, we wished to test a prediction from our KADO observations: that a slow-folding mutant septin would display distinct chaperone interactions relative to the WT allele. We previously showed that the D182N substitution in the GTP-binding pocket of septin Cdc10 renders the mutant protein unable to compete with WT Cdc10 for incorporation into septin complexes, and increases association with the chaperones Hsp104 and Ydj1, according to cofractionation and coprecipitation using cellular lysates (Johnson et al. 2015). To compare chaperone interactions using BiFC, we introduced the D182N mutation into the Cdc10-V_C strain and mated with strains expressing V_N-tagged chaperones.

In no case did we observe fluorescence in septin rings, which presumably reflects KADO-mediated exclusion of the mutant septin from septin complexes, and instead for some chaperones intracellular fluorescence was observed in other locations, including diffusely throughout the cells or in puncta (Figure 1B and data not shown). To compare chaperone interactions between

WT Cdc10 and Cdc10(D182N), we measured intracellular fluorescence using cell outlines, which mostly ignored cortical septin ring signals in WT cells (Supplementary Figure S1C). Whereas WT Cdc10-V_C generated robust signal with Gim3-V_N, almost no fluorescence was detected with Cdc10(D182N)-V_C (Figure 1, C and D). Due to a lack of discrete fluorescence signal, we had not previously called Gim5, another prefoldin subunit, as a septin interactor (Table 1), but quantification revealed diffuse intracellular fluorescence with Cdc10-V_C that decreased drastically for Cdc10(D182N)-V_C (Figure 1, C and D). Conversely, little to no BiFC signal was found in cells coexpressing Cdc10-V_C and Cct6-V_N (Figure 1, B–D), in agreement with our qualitative calls based on discrete signals (Table 1), but Cdc10(D182N)-V_C generated much higher signals, often visible as multiple puncta per cell (Figure 1, B–D). BiFC signal decreased drastically for the cytosolic Hsp90 isoform Hsp82, but not the more highly expressed isoform Hsc82 (Supplementary Figure S1D). BiFC signal also decreased for Ssb2 and Zuo1 (Figure 1, C and D), which comprise an Hsp70–Hsp40 pair within the ribosome-associated complex (RAC) of chaperones that engage nascent polypeptides and promote cotranslational folding (Gautschi et al. 2002; Preissler and Deuerling 2012; Zhang et al. 2017). For the Hsp40 chaperone Ydj1 the change in BiFC signal was more complex. Two populations of cells, differing in the intensity of BiFC fluorescence, were apparent in cultures of each genotype, but the difference was exaggerated by the D182N mutation in Cdc10, with about half of the cells exhibiting almost no signal and the other half having signal higher than the median signal for WT Cdc10 (Figure 1, B–D). Since we measured integrated signal density, we considered that differences in cell size could indirectly alter signals between genotypes, but when we corrected for cell size the same changes were still apparent (Supplementary Figure S1E and data not shown). Finally, Hsp104 BiFC signal was higher with Cdc10(D182N) (Figure 1, C and D),

recapitulating our published biochemical results (Johnson *et al.* 2015). To gauge statistical significance, effect size measurements for most of these differences are provided in Supplementary Figure S1F.

Encouragingly, many of the BiFC differences we saw linked directly to our previous functional studies. The prefoldin subunit Gim3 is required for efficient KADO of Cdc10(D182N), as Cdc10(D182N)-GFP localizes to septin rings in a subset of *gim3Δ* haploid cells coexpressing WT Cdc10 (Johnson *et al.* 2015). Ydj1 is also required for Cdc10(D182N) KADO and Ydj1 overexpression inhibits the proliferation of *cdc10(D182N)* cells (Johnson *et al.* 2015). Hsp104 is dispensable for septin KADO but Hsp104 overexpression inhibits the function of mutant septins subject to KADO (Johnson *et al.* 2015). We note that the decreases in Cdc10 interactions with Ydj1 and prefoldin subunits upon introduction of a mutation predicted to affect folding state are qualitatively similar to those observed with WT Cdc10 in cells cultured at 37°. These results are consistent with a model in which changes in the folding pathway of Cdc10(D182N) compared with WT Cdc10 correspond to changes in the identity and/or duration of the interactions made with cytosolic chaperones.

To ask if these observations with Cdc10 could be extended to another slow-folding mutant septin, we tested Cdc3(G365R), which we have previously shown is slower to incorporate into septin complexes even at a temperature permissive for function and in the absence of a WT allele of *CDC3* (Schaefer *et al.* 2016). We used a haploid strain carrying an untagged copy of the *cdc3(G365R)* allele at the *CDC3* locus and introduced a V_C-tagged allele of *cdc3(G365R)* on a low-copy plasmid, or WT *CDC3* as a control. We then mated this strain with haploid strains carrying selected V_N-tagged chaperones. This strategy allowed the tagged mutant septin to compete with the substoichiometric molecules of untagged WT Cdc3 and successfully localize to septin rings, as evidenced by bud neck fluorescence in cells coexpressing Hsp82-V_N (Figure 1D). That Cdc3(G365R)-V_C showed clear BiFC signal with Hsp82-V_N suggests that the decrease in Cdc10(D182N)–Hsp82 signal (Figure 1, C and D) may be specific to that mutant septin. Examination of septin ring fluorescence in cells expressing V_N-tagged Ydj1 revealed a decrease in BiFC signal for Cdc3(G365R)-V_C compared with Cdc3-V_C (Figure 1D), consistent with our results for Cdc10(D182N) and the decrease in Ydj1 interaction with WT Cdc3 observed at 37°. In summary, among the changes in Cdc10–chaperone interactions observed by BiFC upon introduction of a mutation predicted to slow Cdc10 folding are the two chaperones (Gim3 and Ydj1) that we have already shown to be functionally required for septin KADO, and the two chaperones (Hsp104 and Ydj1) for which we previously found genetic and biochemical evidence of increased physical associations with the mutant septin (Johnson *et al.* 2015). We conclude that BiFC is a useful tool to identify candidate chaperones whose expression can influence the function of misfolded mutant proteins.

Coexpression of WT p53 fails to rescue the folding defects of the p53(V272M) mutant at high temperature

Having used mutant septins to establish BiFC as a useful tool, we wanted to identify differential chaperone interactions with mutant alleles of p53. However, our KADO model does not require chaperone interactions (Schaefer *et al.* 2016). Hence we first addressed other mechanisms that could prevent certain p53 mutants from acting dominantly to inhibit the function of the WT.

It was previously proposed (Dearth *et al.* 2007) that the reason some misfolded p53 mutants are recessive is because their proper folding is restored via interaction with properly folded WT p53 molecules in the context of "mixed" hetero-tetramers. The V272M mutant adopts a non-native conformation in a TS manner (North *et al.* 2002; Blanden *et al.* 2020) and acts recessively when coexpressed with WT p53 in yeast cells harboring a *URA3* reporter gene containing p53 binding sites in the promoter region (Brachmann *et al.* 1996; Dearth *et al.* 2007; see Figure 3). To ask if WT p53 is able to "chaperone" the proper folding of p53(V272M), we used a split-dihydrofolate reductase (split-DHFR) assay (Pittman *et al.* 2012). Here, p53 is fused between two fragments of DHFR and only folded p53 supports DHFR activity, manifested as proliferation by *dfr1Δ* yeast cells on medium lacking exogenous dTMP (Figure 2A). As shown in Figure 2B, *dfr1Δ* cells expressing a split-DHFR construct with p53(V272M) or p53(Y220C), another recessive and TS mutant (Dearth *et al.* 2007), barely proliferated at 37° on medium lacking dTMP. Equivalent constructs with WT or p53(R273H), a contact mutant that folds normally but cannot interact with DNA (Bullock *et al.* 1997), supported faster colony growth at all temperatures (Figure 2B). Coexpressing untagged WT p53 had no obvious effect when proliferation was assessed using colony growth on solid medium (Figure 2C). We also used a liquid culture growth assay and here observed only a very slight effect for Y220C (Figure 2D). Based on these data, we think folding rescue via interaction with WT p53 is unlikely to explain why the mutants do not act dominantly to interfere with WT function.

High temperature inhibits p53(V272M) nuclear localization and coassembly with WT p53

We next asked if kinetic delays during *de novo* synthesis and/or folding of p53(V272M) relative to WT p53 might prevent V272M mutant molecules from coassembling with WT molecules into dysfunctional oligomers, akin to the KADO phenomenon we observed for septins. Oligomerization buries a nuclear export signal and ensures nuclear p53 localization (Stommel *et al.* 1999). Similar to how we monitored the kinetics of septin synthesis, folding and assembly by asking how long it takes a fluorescentlytagged septin to reach the septin ring at the bud neck (Schaefer *et al.* 2016), we monitored nuclear mKate2 signal after induction of mKate2-tagged p53 or p53(V272M). Since steady-state nuclear levels of WT p53 and p53(V272M) were equivalent at 24° (Figure 3A, 10-h timepoint and data not shown), we performed our experiments at this temperature. Our quantitative analysis demonstrated similar kinetics of nuclear accumulation for both WT and p53(V272M) (Figure 3A). Effect sizes with associated 95% C.I. for these and other quantifications of p53 fluorescence can be found in Supplementary Figure S2. These results suggest that at low temperature mutant p53 is not significantly delayed relative to WT p53 in achieving the oligomerization-competent conformation required to reach the nucleus.

By contrast, nuclear localization of p53(V272M)-mKate2 was reduced at 30° and greatly reduced at 37° (Figure 3B). Temperature had a much smaller effect, if any, on nuclear levels of WT p53 and the "contact" mutant R273H (Figure 3B). These data point to a failure in nuclear localization as a major cause of p53(V272M) dysfunction at high temperature. The inability of V272M to dominantly interfere with WT p53 when the two alleles are coexpressed may reflect a reduced ability of V272M to coassemble with WT molecules into "mixed" oligomers wherein the mutant perturbs WT function. If WT p53 interacts poorly with

p53(V272M) at 37° that would additionally explain the results of our split-DHFR experiments.

We next used BiFC to test for p53–p53 interactions in living cells, using p53-mKate2-V_C and p53-mKate2-V_N constructs previously validated in mammalian cells (Gaglia and Lahav 2014). We quantified nuclear signal for total p53 (mKate2 fluorescence) and for p53–p53 BiFC (Venus fluorescence) at 30° and 37°. Whereas total nuclear p53 and BiFC signals indicative of p53–p53 interactions were indistinguishable for WT–WT and WT–R273H at 37°, for WT–V272M both total nuclear p53 and BiFC signals were reduced (Figure 3C). Since WT p53 also contributed to nuclear signal, this means that at 37° coexpression of the V272M mutant partially inhibited the nuclear localization of WT p53. By normalizing nuclear BiFC signal to total nuclear p53 signal, we found that the relative proportion of nuclear p53 present as "mixed" oligomers was much higher for WT–V272M than WT–WT or WT–R273H (Figure 3C). These data indicate that at 37° only a small number of V272M molecules are able to interact with WT p53 and remain the nucleus, supporting a model in which at high temperature V272M mostly fails to fold into an oligomerization-competent conformation and thus cannot inhibit WT p53 function.

In previous studies, including during cell-free translation *in vitro* (Nicholls *et al.* 2002), p53 dimerized cotranslationally (Gaglia and Lahav 2014) such that tetramers assemble from dimers composed of two monomers encoded by the same mRNA. Thus distinct alleles do not "mix" in the dimer form but rather in the tetramer form only. We tried to assess the extent to which cotranslational p53 dimerization might contribute to the interaction (or lack thereof) between WT p53 and p53(V272M), but in our yeast system the mutants postulated to block oligomerization before the dimerization (L344P) or tetramerization (L344A) step (Gaglia *et al.* 2013; Gaglia and Lahav 2014) did not reliably prevent interaction between differentially tagged p53 alleles, particularly in a BiFC context (Supplementary Figure S3). Thus we were unable to distinguish between cotranslational and posttranslational mechanisms of dimerization or determine the point at which oligomerization fails in the V272M mutant.

The V272M mutation converts the dominant R273H mutant to a recessive form

If p53(V272M) is recessive because it misfolds and fails to interact with WT p53, and p53(R273H) is dominant because it interacts with WT p53 to form dysfunctional tetramers, then introducing the V272M mutation should sequester the R273H mutant in the cytosol and render it recessive. Indeed, quantification of nuclear fluorescence revealed that nuclear localization of p53(V272M R273H) was diminished at 30° and greatly diminished at 37°, patterns indistinguishable from that of p53(V272M) (Figure 3B). Like p53(R273H), when expressed alone p53(V272M R273H) was transcriptionally inactive at all temperatures tested (Figure 3, D and E). At 30°, both p53(R273H) and p53(V272M R273H) dominantly inhibited WT p53 function (Figure 3F). However, at 37° p53(V272M R273H) was unable to inhibit WT function (Figure 3F), consistent with our prediction. These data point to temperature-induced misfolding and cytosolic sequestration as the major mechanisms by which the V272M mutation perturbs oligomerization and compromises p53 function.

Cytosolic chaperone–p53 interactions in living cells

Given the evidence that misfolding of p53 mutants is responsible for dysfunction at high temperatures (reviewed in Bullock and Fersht 2001) and drives prolonged associations with at least three kinds of cytosolic chaperones (Blagosklonny *et al.* 1996; Sepehrnia *et al.* 1996; Singh *et al.* 2010; Wiech *et al.* 2012), we used our BiFC approach to systematically identify p53–chaperone interactions. We predicted that the conformationally unstable p53(V272M) would have altered chaperone interactions relative to WT p53 or the "contact" mutant p53(R273H). We used 28 of the same V_N-tagged chaperones as with septins, paired with the p53-mKate2-V_C fusion from the p53–p53 BiFC experiments described above. (Note that the V_C tag here is slightly larger than the V_C tag used with septins.)

We identified interactions between p53 and numerous cytosolic chaperones (Figure 4A, Supplementary Figure S4A, and summarized in Table 2). To account for differential proteasomal degradation of p53 mutants (Singh *et al.* 2010), we used the mKate2 tag to normalize the p53-chaperone BiFC signal (Venus) relative to total p53 signal (mKate2), which revealed increased interactions between p53(V272M) and many chaperones relative to WT p53 and p53(R273H) (Figure 4B). Several chaperones—Hsp82, Ssb1, Sis1, and Ydj1—demonstrated increases in p53(V272M) interaction that were obvious even before normalization (raw values in Supplementary Figure S4B).

With the exception of Cct7 and Hsp12, and Hsp104, which generated decreased and increased BiFC signal with p53(R273H) compared with WT, respectively, most chaperones interacted in similar ways with p53(R273H) and WT p53, whereas p53(V272M) displayed multiple distinct interactions (Figure 4B and Supplementary Figure S4B). p53(R273H) specifically abolishes contact with DNA without global conformational consequences (Ang *et al.* 2006). On the other hand, p53(V272M) causes misfolding and conformational instability (North *et al.* 2002; Blanden *et al.* 2020). These observations are consistent with a model in which chaperones recognize specific, exposed sequences in p53 that are largely buried in the native fold. The V272M mutation results in prolonged exposure of these sequences and thus more opportunities for cytosolic chaperone engagement.

In some cases, we also saw differences in BiFC signal localization. At 30°, the temperature at which we cultured cells prior to microscopic examination, the mKate2-V_C-tagged p53 alleles differed from each other in their localization even when no V_N-tagged chaperone was expressed. WT p53 and the R273H mutant were seen in both the cytosol and the nucleus, whereas the V272M mutant was found almost exclusively in the cytosol (Supplementary Figure S4A, "No BiFC Control"). These observations agree with prior cell fractionation experiments in mammalian cells, in which WT p53 and p53(R273H) were found almost exclusively in the nuclear fraction, regardless of temperature (Zhang *et al.* 1994) whereas p53(V272M) showed a distinct shift toward the cytosolic fraction even at low temperatures (Dearth *et al.* 2007). Most p53–chaperone BiFC signals were in the cytosol, either diffusely, as puncta, or a mixture of both signal types (Table 2). Hsp70 chaperones Ssb1 and Ssb2 generated diffuse cytosolic signal whereas Ssa2, Cct7, and Hsp104 generated exclusively punctate signals (Table 2, Figure 4A, and Supplementary Figure S4A). Multiple p53–Cct7 puncta were seen in some cells (Figure 4A), clearly distinguishing them from septin–Cct7 puncta. Chaperones producing a mixture of both diffuse and punctate cytosolic signal include the Hsp90 isoforms Hsp82 and Hsc82 (with brighter and more numerous puncta for Hsc82) and the Hsp40 family members Sis1, Ydj1, and Zuo1 (Table 2, Figure 4A, and Supplementary Figure S4A). Sis1 and Hsp12 were unique in producing nuclear signal in addition to cytosolic fluorescence (Figure 4A and Supplementary3 Figure S4A). Sis1 generated nuclear signal for WT and p53(R273) but essentially none for p53(V272M) (Figure 4A).

Table 2. p53–chaperone interactions assayed by BiFC

Chaperone (family)	Major cellular compartment (minor)[a]	p53 BiFC interactions[b]	Published evidence[c]
Ssa1 (Hsp70)	Cytosol (Nucleus)	—	P, F (reviewed in Zylicz *et al.* 2001; Wawrzynow *et al.* 2018), F for yeast Ssa2 (Singh *et al.* 2010)
Ssa2 (Hsp70)	Cytosol (Mitochondria)	WT•, V272M•, and R273H•	
Ssa3 (Hsp70)	Cytosol	—	
Ssa4 (Hsp70)	Cytosol (Nucleus)	—	
Ssb1 (Hsp70)	Cytosol	WT°, V272M°, and R273H°	
Ssb2 (Hsp70)	Cytosol	WT°, V272M°, and R273H°	
Sse2 (Hsp70)	Cytosol	—	
Ssz1 (Hsp70)	Cytosol	—	
Apj1 (Hsp40)	Cytosol (Nucleus, Mitochondria)	—	P, F (reviewed in Wawrzynow *et al.* 2018)
Djp1 (Hsp40)	Cytosol	—	
Jjj1 (Hsp40)	Cytosol (Nucleus, Mitochondria)	—	
Jjj2 (Hsp40)	Cytosol (Nucleus)	—	
Sis1 (Hsp40)	Cytosol (Nucleus)	WT °•*, V272M°•, and R273H °•*	
Swa2 (Hsp40)	Cytosol (ER Membrane)	—	
Ydj1 (Hsp40)	Cytosol (ER Membrane)	WT°•, V272M°•, and R273H°•	
Zuo1 (Hsp40)	Cytosol (Nucleus)	WT°•, V272M°•, and R273H°•	
Hsp12 (small)	Cytosol (Nucleus)	WT°*, V272M°*, and R273H°*	P for human αB-crystallin (Liu *et al.* 2007) and P, F for yeast Hsp26 (Singh *et al.* 2010)
Hsp26 (small)	Cytosol (Nucleus)	—	
Hsp31 (small)	Cytosol	—	
Hsp32 (small)	Cytosol	—	
Hsp33 (small)	Cytosol	—	
Hsp42 (small)	Cytosol	—	
Sno4 (small)	Cytosol	—	
Hsp82 (Hsp90)	Cytosol (Mitochondria)	WT°•, V272M°•, and R273H°•	P, F (reviewed in (Wawrzynow *et al.* 2018))
Hsc82 (Hsp90)	Cytosol	WT°•, V272M°•, and R273H°•	
Hsp104 (AAA+)	Cytosol (Nucleus)	WT•, V272M•, and R273H•	F in yeast (Singh *et al.* 2010)
Cct7 (CCT/TRiC; Type II Chaperonin)	Cytosol	WT•, V272M•, and R273H•	P, F (Trinidad *et al.* 2013)
Gim 3 (Prefoldin/GimC)	Cytosol	—	

a Our interpretation of the literature regarding the major subcellular localization for the chaperone in question, with minor localizations given in parenthesis.
b Measured at 30°. "—," no discrete signal. "°," fluorescence signal appeared as diffuse cytosolic; "•," punctate cytosolic signal; "°•," both diffuse and punctate cytosolic signal; "*," nuclear signal.
c (P), physical; (F), functional.

By monitoring the mKate2 signal, we found several cases in which coexpression of a V_N-tagged chaperone altered the localization of mKate2-V_C-tagged p53 (Figure 4A and Supplementary Figure S4A). These observations are consistent with a model in which Venus reconstitution trapped the p53 molecules in the location where the chaperone is normally found. Nuclear mKate2 signal for p53(V272M) in cells coexpressing Hsp12-V_N is a particularly striking example (Supplementary Figure S4A). In all cases, the Venus signal colocalized with the p53 mKate2 signal in the "new" location, further arguing that BiFC events were responsible (Figure 4A and Supplementary Figure S4A). We interpret these data as evidence that, just as in septin–chaperone BiFC, making permanent an otherwise transient interaction incites a localization "tug-of-war." For most septin–chaperone interactions, the septin wins; for all p53–chaperone interactions, the chaperone wins. Only in the case of a subset (∼5%) of p53(V272M) cells did p53 localize as puncta in the absence of a coexpressed VN-tagged chaperone (not shown). When expressed in yeast, WT p53 forms cytoplasmic puncta in response to various stresses (Park *et al.* 2021). Accordingly, we suspect that the BiFC puncta arise from p53 misfolding and abnormal oligomerization driven by prolonged association with the tagged chaperone. The results described above point to a number of chaperones as compelling candidates to influence the function of mutant alleles of p53.

Overexpression of specific chaperones inhibits p53(V272M) function

Differences in chaperone engagement might explain functional differences between p53(V272M) and WT p53 if a chaperone sequesters the mutant protein in a nonfunctional state. We asked if the function of p53 could be aggravated by chaperone overexpression at a permissive temperature, focusing on the chaperones identified by our BiFC experiments. Plasmids encoding chaperones under control of a galactose-inducible promoter were introduced into a diploid *URA3* reporter strain also carrying a plasmid encoding untagged WT p53 or p53(V272M) under control of a constitutive promoter. Various cytosolic chaperones impeded the transcriptional function of p53(V272M) and, to a generally lesser degree, WT p53 (Figure 5A). Exceptions included Hsf1ΔN, a constitutively active version of the major heat shock transcriptional regulator (Park *et al.* 2006), where WT p53 and p53(V272M) behaved similarly. By contrast, Hsf1ΔN, like expression of specific individual chaperones, inhibited the proliferation of cells with the *cdc10(D182N)* septin mutation (Johnson *et al.* 2015). Hsp90 isoforms Hsp82 and Hsc82 slightly but equivalently impeded mutant p53(V272M) relative to WT p53 although the intensity of signal and number of puncta were increased for endogenous levels of Hsc82 in BiFC experiments. Both Hsp90 isoforms were expressed at similar levels, as assessed by immunoblotting (Figure 5B).

Since the transcriptional activation function we monitor here requires nuclear p53, one way chaperone engagement might inhibit p53(V272M) function is via cytosolic sequestration. We quantified nuclear *vs* cytosolic p53(V272M)-mKate2-Venus signal in micrographs and found that in most cases chaperone overexpression decreased the nuclear/cytosolic ratio of p53(V272M), with the exception of Ydj1 where the ratio was preserved (Figure 5C). Notably, in this imaging-based approach, cytosolic p53(V272M) levels sometimes also decreased along with nuclear levels relative to empty vector (Supplementary Figure S5, A and B), as illustrated for Sis1 (Figure 5D). However, when we tested Sis1 overexpression

by immunoblotting, we saw no clear difference in total p53(V272M) levels relative to the empty vector control (Figure 5D). Our imaging-based quantification may underestimate total cytosolic levels, since we excluded what is likely vacuolar p53 signal seen in some chaperone-overexpressing cells (e.g., Sis1 and Zuo1; Figure 5E). We interpret these data as evidence that overexpression of specific chaperones sequesters p53(V272M) outside the nucleus and impedes transcriptional activation.

Overexpression of some chaperones inhibited colony growth in general, even when we did not select for p53 function, and this effect was independent of the p53 allele expressed (Figure 5A). Overexpression of these same chaperones in cells not coexpressing p53 has no such effect (Sopko et al. 2006; Johnson et al. 2015). High-level p53 expression is toxic to yeast and is thought to involve p53 binding to endogenous yeast genes and thereby perturbing essential gene expression (Inga and Resnick 2001; Leão et al. 2013; Park et al. 2021). We noticed a trend in which the chaperones with stronger effect on nonselective growth (i.e., those that induced the most p53 "toxicity") had more p53(V272M) in the nucleus (Figure 5, A and C and Supplementary Figure S5, A and B). Conversely, the chaperones that specifically inhibited p53(V272M) transcriptional activation function and most strongly decreased the levels of p53(V272M) in the nucleus (Hsp31, Ssa4, Hsp26, and Cct7) had little to no effect on nonselective growth (Figure 5, A and C and Supplementary Figure S5, A and B). Although the details of the underlying mechanism are beyond the scope of this work, these results support the idea that p53 toxicity in yeast requires nuclear localization. However, our findings further suggest that canonical transcriptional activation function is dispensable for toxicity, and that whatever function is responsible can be modulated by chaperone expression.

Chaperone inhibition liberates p53 from cytosolic compartmentalization

If association with a specific chaperone mediates cytosolic sequestration, then inhibiting the ability of that chaperone to bind p53 should allow more p53 to reach the nucleus. Indeed, when we inhibited Hsp90 function using radicicol (Sharma and Masison 2011), nuclear levels and nuclear/cytosolic ratios increased for WT p53 and all variants (Supplementary Figure S5, C and D and Figure 6A). As assessed by immunoblotting, total p53 levels were not detectably changed between DMSO- and radicicol-treated cells (Figure 6B). Reminiscent of chaperone-overexpressing cells, we also observed what is likely vacuolar p53 signal in cells treated with radicicol but not with DMSO (Figure 6C); this extranuclear signal was not included in our quantification of cytosolic p53 (Supplementary Figure S5, C and D). These findings are consistent with other studies with mammalian cells in which pharmacological Hsp90 inhibition increased nuclear localization of a different p53 mutant (Whitesell et al. 1998).

Notably, in that study Hsp90 inhibition did not improve the function of the mutant p53 (Whitesell et al. 1998). To ask if the liberation of nonfunctional mutant p53 from chaperone sequestration might increase the ability of the V272M mutant to dominantly interfere with nuclear p53 function at 37°, we used FOA to select against activity of the URA3 reporter, but saw only a very slight apparent increase in colony growth in the presence of radicicol, and this increase occurred regardless of whether or not the cells coexpressed p53(V272M) (Supplementary Figure S6A). Considering that even WT p53 is conformationally labile and often samples nonfunctional conformations (Hainaut et al. 1995; Cañadillas et al. 2006), this result might suggest that Hsp90 inhibition allows molecules of WT p53 in nonfunctional conformations to translocate to the nucleus, where they cannot activate transcription but may dominantly interfere with the function of any properly folded molecules. To test if a colony-color-based reporter might be more sensitive, we coexpressed WT p53 with p53(R273H) in a strain in which p53 activity promotes expression of the ADE2 gene (Supplementary Figure S6B). However, diminished color development at 37° precluded analysis of dominant inhibition (Supplementary Figure S6D). Thus the functional consequences of releasing p53 from cytosolic chaperone sequestration remain unclear.

Discussion

Chaperone binding to a misfolded protein is widely assumed to either promote proper folding or protect cells from adverse consequences of irreversibly misfolded proteins. Accordingly, chaperone upregulation or overexpression should rescue mutant protein function. However, in some cases chaperones "inappropriately" sequester otherwise functional proteins, such as the ΔF508 mutant allele of CFTR, the most common mutation causing human cystic fibrosis (Amaral 2006; Balch et al. 2011; Lopes-Pacheco et al. 2015). Conversely, some mutant proteins can fold well enough to hetero-oligomerize with WT partner proteins but carry substitutions that "poison" the function of the hetero-oligomer. Here, chaperone sequestration can render recessive an otherwise dominant-negative mutant. We aimed to developed tools for identifying chaperones that differentially engage misfolding-prone mutant proteins, and use them to test if chaperone association affects the function and dominant-negative effect of a misfolding-prone mutant of p53.

Our BiFC approach identified differential septin–chaperone interactions that matched results from our prior functional studies (Johnson et al. 2015). Only 2 of 11 intended negative controls, Sec63 and Pam18, generated detectable septin BiFC signal (Table 1). We suspect that, in addition to its role in translocating polypeptides across the ER membrane (Ng and Walter 1994), the Hsp40 family member Sec63 transiently associates with many cytosolic proteins (including septins), only some of which are ultimately threaded into the ER lumen. Consistent with this interpretation, Sec63-V_C interacts with "free" V_N (Kim et al. 2019). Hence, in retrospect Sec63 was not a good negative control. The mitochondrially localized chaperone Pam18 interacted only with Cdc3 and only at 37° (Table 1). Although interactions between Cdc12 and Pam18 and between Cdc3 and Hsp78, another mitochondrial chaperone, were reported in high-throughput genetic (Davierwala et al. 2005) and two-hybrid (Wang et al. 2012) screens, we doubt that these interactions are biologically meaningful.

Although many cytosolic chaperones are highly abundant proteins thought to interact with a wide range of proteins, only some interacted with septins in our assay. If chaperones merely engaged the V_C portion of the septin-V_C fusions, and not the septins themselves, we might expect a much broader spectrum of cytosolic chaperone BiFC interactions. For example, the Hsp70 Ssa1 is the most abundant chaperone in the cytosol of unstressed yeast cells (Brownridge et al. 2013), but it did not interact with any septin at any temperature. Conversely, its much less abundant, 98%-identical paralog, Ssa2, interacted with all five septins (Table 1). Other studies using the same Ssa1-V_N strain were able to detect BiFC interactions with other proteins (Sung et al. 2013), demonstrating that the Ssa1-V_N fusion is functional. Ssa1 and Ssa2 also have distinct functions in prion propagation (Allen et al. 2005) and the vacuolar import and degradation pathway of gluconeogenic enzyme regulation (Brown et al. 2000; Sharma and Masison

2011). As another example, the Hsp70 Ssz1 forms a ribosome-associated complex with Zuo1 and the other Hsp70s Ssb1 or Ssb2, but Ssz1 appears to have lost its ability to bind nascent substrate polypeptides (Huang *et al.* 2005). In agreement with this idea, we found that Zuo1-V_N and Ssb1-V_N, but not Ssz1-V_N, interacted with V_C-tagged septins (Table 1). Thus, we are confident that our BiFC results reveal specific associations, not nonspecific interactions or promiscuous encounters.

A previous study using a trimolecular fluorescence complementation (TriFC) assay to identify septin-interacting proteins in living yeast cells specifically tested interactions with Hsp82 as a negative control, and found none (Finnigan *et al.* 2016). We suspect that the septin–Hsp82 interactions we see with BiFC reflect the relatively large sizes of the V_C and V_N tags, the linkers between them, and the C termini of the septins and chaperones to which they were fused, compared with the very small (20–21 residues) tags and linkers (18–33 residues) used in the TriFC system (Finnigan *et al.* 2016). The TriFC study demonstrated that the small tags and short linkers limit signal generation to interactions occurring within a short distance, such that only septins adjacent to each other in the septin hetero-oligomeric complex generate TriFC signal (Finnigan *et al.* 2016). In our BiFC system, all septins interact with all septins (our unpublished observations). Accordingly, Hsp82 could probably interact with any part of a septin protein and generate BiFC signal, but would likely need to bind nearby the N or C terminus in order to generate TriFC signal. Since our KADO model predicts that chaperones recognize septins with misfolded GTPase domains (Johnson *et al.* 2015), which are formed primarily by residues in the middle of septin proteins, using a split-fluorophore approach to identify septin–chaperone interactions may require larger tags and longer linkers.

Accordingly, the drop in specific chaperone BiFC signals we observed for mutant septins relative to their WT counterparts does not necessarily mean those chaperone–septin interactions no longer occurred. Differences in conformation or exposure of chaperone binding sites for a mutant septin may increase the physical distance between the C-terminal V_C tag on the septin and the C-terminal V_N tag on the chaperone beyond the BiFC threshold. These differences may explain diminished BiFC signals for chaperones whose deletions (Ydj1 and Gim3) perturb septin KADO, and whose overexpression (Ydj1) impedes mutant septin function.

The changes in chaperone interactions upon septin mutation were similar to changes for WT septins at high temperature (Table 1). Certain chaperones may recognize non-native conformations that WT proteins only sample at high temperature but mutant proteins readily adopt at low temperature. Recent work on mammalian Hsp90, for example, suggests that client binding depends on the combined probabilities of partial client unfolding, capture by Hsp70 of a transiently exposed site, and further unfolding events that expose adjacent client regions for capture by Hsp90 in complex with cochaperones (Wang *et al.* 2020). The mutations we examined could promote any or all of these events. We chose V272M as a representative example of a p53 mutant with global structural instability and temperature-aggravated misfolding, and we have no reason to suspect that other p53 mutants with similar structural defects (*e.g.*, manifested as temperature sensitivity) would behave differently.

Alternatively, the presence of a mutant protein might itself alter chaperone expression in ways that mimic the effects of high temperature, such that a different repertoire of chaperones is available for interaction, independent of protein conformation *per se*. Indeed, expression of mutant p53 in yeast cells was sufficient to alter chaperone expression without an increase in temperature (Singh *et al.* 2010). The BiFC tags themselves may also alter chaperone expression: we detected BiFC signals with WT septins for chaperones whose expression in nonstress conditions is normally very low (*e.g.*, Ssa3; Werner-Washburne *et al.* 1987, Table 1). The V_C tag itself did not drive chaperone binding; however, since p53-V_C did not interact with Ssa3-V_N (Table 2).

Whereas chaperone binding at the septin–septin G interface and competition with other septins for interaction there is consistent with predictions from our KADO model for mutant septins, most known chaperone binding sites in WT p53 are found in the structurally labile DBD (Fourie *et al.* 1997; Müller *et al.* 2004), as opposed to the oligomerization domain. If the same sites mediate chaperone binding to p53(V272M), then it seems less likely that chaperone binding directly blocks oligomerization by mutant p53 and, since oligomerization buries the p53 nuclear export signal, indirectly promotes cytosolic sequestration. The three p53 nuclear localization signals are all located near the C terminus and outside the DBD (Shaulsky *et al.* 1990), hence direct occlusion of these sequences by chaperone binding is also an unlikely mechanism of cytosolic sequestration.

Instead, chaperone binding to the p53 DBD could inhibit nuclear localization of p53 in other ways. In mammalian cells, p53 nuclear localization is controlled by many factors not present in yeast, including the protein MDM2, intermediate filaments, and dynein-mediated transport along microtubules (reviewed in O'Brate and Giannakakou 2003). Nonetheless, the same NLS and NES sequences that control p53 nuclear localization in mammalian cells also control p53 nuclear localization when expressed in yeast (Godon *et al.* 2005). Binding of mammalian Hsp70–Hsp40 to the WT p53 DBD alters its conformation to disfavor DNA binding (Boysen *et al.* 2019), but an inability to bind DNA cannot explain the cytosolic sequestration of p53(V272M) because the contact mutant R273H does not have the same problems with nuclear retention (Figure 3B). We suspect that cytosolic chaperone–p53 complexes are retained in the cytosol because chaperone binding stabilizes a conformation of p53 in which the NLS is unavailable for proper interaction with the nuclear import machinery. Indeed, experiments in mammalian cells with a different TS p53 mutant, C135V, suggested that at high temperature binding of cytosolic Hsp70 chaperones to the mutant p53 renders the NLS inaccessible without directly occluding it (Akakura *et al.* 2001). p53 expressed in yeast can adopt several forms with distinct localization patterns—both punctate and diffuse, and in the cytosol, vacuole, or nucleus—some of which can be stably propagated in prion-like ways, suggesting conformational changes in p53 drive the changes in localization (Park *et al.* 2021). Since most of the chaperones we overexpressed are normally found diffusely in the cytosol, we think that the distinct patterns of p53 mislocalization outside the nucleus upon overexpression of distinct chaperones (punctate, diffuse, likely vacuolar) may have more to do with the conformation of p53 resulting from chaperone interaction than with chaperone binding *per se*. Along the same lines, the p53 we saw localized to the presumptive vacuole upon Hsp90 inhibition probably represents p53 liberated from Hsp90 but captured by other chaperones and ultimately excluded from the nucleus.

Our findings that overexpression of any one of many distinct chaperones specifically inhibited the *function* of p53(V272M) suggest that cytosolic sequestration was sufficient but not necessary for functional inhibition. For example, Ydj1 overexpression inhibited p53(V272M) function but actually increased nuclear p53 levels (Figure 5A, Supplementary Figure S5, A and B). Hence some conformations of p53 are presumably able to enter and remain in

the nucleus but are unable to function there properly. From a broader perspective, these functional data with p53(V272M) add to our previous results with mutant septin function (Johnson et al. 2015) and run counter to the idea that elevated chaperone expression generally improves the folding and function of mutant proteins. Although chaperone "assistance" with mutant p53 folding and function has been suggested in studies with other mutants expressed in yeast (including, interestingly, R273H; Singh et al. 2010), our data demonstrate that overexpression of the same chaperone (Ssa2) was inhibitory to V272M function (Figure 5A). This discrepancy may point to differences in how chaperone binding alters the folding of a contact mutant (R273H) vs a conformational mutant (V272M). The extent and context of chaperone "overexpression" may also be important: the effect of Ssa2 on p53(R273H) was observed not by directly overexpressing Ssa2 but by adding ethanol, which indirectly induced Ssa2 (Singh et al. 2010). Similarly, some of the chaperones that had a functional effect on p53(V272M) were negative for BiFC interaction (i.e., Ssa4, Hsp26, and Hsp31). One potential explanation for this discrepancy is the high GAL1/10-driven chaperone expression we used in the functional assays, compared with endogenous chaperone levels in BiFC.

Another key point of comparison between our present results and those of prior studies is the effect of chaperone inhibition/deletion. In our earlier septin studies, deleting specific chaperone-encoding genes liberated mutant septins from apparent sequestration and allowed them to oligomerize with other, WT septins (Johnson et al. 2015). We focused on Ydj1 and Gim3 because published positive genetic interactions between ydj1Δ or gim3Δ and TS septin alleles hinted at improved function of the mutant septin when the chaperone was removed (Costanzo et al. 2010). In fact, however, the double-mutant cells were no more functional than either single mutant; they were merely less dysfunctional than one would have expected if each mutation independently compromised proliferation (Costanzo et al. 2010). Our finding that the Hsp90 inhibitor radicicol promotes nuclear localization of mutant p53 is conceptually similar, if we interpret it as p53 liberation from cytosolic chaperone sequestration but without fixing the folding problems that compromise function.

Indeed, our observation that radicicol also drives WT and R273H molecules of p53 into the nucleus (Figure 6) may explain the unexplained finding (Godon et al. 2005) that various forms of cellular stress (radiation, cadmium, and mercury) promote localization of p53 to the yeast nucleus. If these stressors (all of which are known to induce the heat shock response) generate misfolded or damaged proteins, those proteins may exceed the sequestration capacity of the cytosolic chaperone machinery, and liberate misfolded p53 molecules to enter the nucleus. Such a mechanism would be reminiscent of the way proteostatic stress liberates Hsf1 from cytosolic Hsp70–Hsp90 sequestration and allows Hsf1 to trimerize, accumulate in the nucleus and activate chaperone gene expression (Morimoto 1998). Not all ways of inhibiting chaperone sequestration have the same effect; however, deleting the gene encoding the small heat shock protein Hsp26 rescues the function of p53(R273H) expressed in yeast (Singh et al. 2010). Presumably, p53(R273H) is able to achieve a functional conformation without Hsp26 assistance, whereas Hsp90 contribution to p53 folding is indispensable.

Finally, our findings do not support a KADO model for the recessive behavior of p53(V272M). KADO predicts delayed arrival of mutant V272M molecules in the nucleus and delayed mixing with WT, together with a recessive phenotype at all temperatures. Instead we observed a thermodynamic blockade on the ability of the vast majority of V272M molecules to reach a conformational state competent for nuclear localization. Sparing of WT inhibition by p53(V272M) and p53(V272M R273H) was only achieved at 37°, a temperature where the mutant was thermodynamically sequestered in the cytosol, rather than simply kinetically delayed in its nuclear arrival. For mutant septins, a poorly defined "window of opportunity" for hetero-oligomerization in the G1 phase of the cell cycle enforces mutant exclusion by KADO (Schaefer et al. 2016). We suspected that cotranslational dimerization might represent a p53 "window of opportunity," whereby a slow-folding mutant would be forced to dimerize post-translationally and miss the chance to form mutant dimers that could mix with WT dimers. However, based on our findings it is unclear if in yeast WT p53 dimerization is cotranslational, and there is likely no kinetic "deadline" by which a p53 molecule must fold in order to properly oligomerize. Taken together, this study highlights key differences between septin oligomerization and p53 oligomerization and the effects of TS mutations and chaperone binding, which help us understand the general principles underlying dominant and recessive mutant phenotypes.

Data availability

Strains and plasmids are available upon request. The authors affirm that all data necessary for confirming the conclusions of the article are present within the article, figures, tables, and supplementary materials. Macros for analyzing fluorescence intensity are available on GitHub (https://github.com/michael-mcmurray/Denney-et-al-G3-2021/).

Supplementary files are available at figshare: https://doi.org/10.25387/g3.14673309. Supplementary Table S1 describes yeast strains used in this study. Supplementary Table S2 lists

oligonucleotides used in this study. Supplementary Table S3 contains plasmids along with construction details used in this study. Supplementary Figure S1 illustrates septin–chaperone BiFC interactions and quantification along with effect size plots and associated 95% C.I. Supplementary Figure S2 contains effect size plots with associated 95% C.I. corresponding to various p53 measurements found in Figures 3, A–C, 4B, 5, C and D, 6A, and Supplementary Figure S3B. Supplementary Figure S3 contains coimmunoprecipitation and BiFC experiments with p53 mutants L344A and L344P. Supplementary Figure S4 illustrates positive p53–chaperone BiFC interactions not included in Figure 4A along with raw BiFC and total p53 values corresponding to data in Figure 4B. Supplementary Figure S5 contains raw nuclear and cytosolic p53 values, along with effect size plots and associated 95% C.I., corresponding to data in Figures 5C and 6A. Supplementary Figure S6 depicts *URA3*- and *ADE2*-based p53 reporters and their utility in detecting dominant effects of p53 mutants.

Conflicts of interest

None declared.

Literature cited

Akakura S, Yoshida M, Yoneda Y, Horinouchi S. 2001. A role for Hsc70 in regulating nucleocytoplasmic transport of a temperature-sensitive p53 (p53Val-135). J Biol Chem. 276: 14649–14657. doi:10.1074/jbc.M100200200

Allen KD, Wegrzyn RD, Chernova TA, Müller S, Newnam GP, *et al.* 2005. Hsp70 chaperones as modulators of prion life cycle novel effects of SSA and SSB on the *Saccharomyces cerevisiae* prion [PSI+]. Genetics. 169:1227–1242. doi:10.1534/genetics.104.037168

Amaral MD. 2006. Therapy through chaperones: sense or antisense? Cystic fibrosis as a model disease. J Inherit Metab Dis. 29:477–487. doi:10.1007/s10545-006-0251-x

Amberg D, Burke D, Strathern J. 2005. Methods in Yeast Genetics: A Cold Spring Harbor Laboratory Course Manual, 2005 ed. Cold Spring Harbor Laboratory Press.

Ang HC, Joerger AC, Mayer S, Fersht AR. 2006. Effects of common cancer mutations on stability and DNA binding of full-length p53 compared with isolated core domains. J Biol Chem. 281: 21934–21941. doi:10.1074/jbc.M604209200

Balch WE, Roth DM, Hutt DM. 2011. Emergent properties of proteostasis in managing cystic fibrosis. Cold Spring Harb Perspect Biol. 3: a004499. doi:10.1101/cshperspect.a004499

Balchin D, Miličić G, Strauss M, Hayer-Hartl M, Hartl FU. 2018. Pathway of actin folding directed by the eukaryotic chaperonin TRiC. Cell. 174:1507–1521.e16. doi:10.1016/j.cell.2018.07.006

Billant O, Blondel M, Voisset C. 2017. p53, p63 and p73 in the wonderland of S. *cerevisiae*. Oncotarget. 8:57855–57869. doi:10.18632/oncotarget.18506

Blagosklonny MV, Toretsky J, Bohen S, Neckers L. 1996. Mutant conformation of p53 translated in vitro or in vivo requires functional HSP90. Proc Natl Acad Sci U S A. 93:8379–8383.

Blanden AR, Yu X, Blayney AJ, Demas C, Ha J-H, *et al.* 2020. Zinc shapes the folding landscape of p53 and establishes a pathway for reactivating structurally diverse cancer mutants. Elife. 9: e61487. doi:10.7554/eLife.61487

Boysen M, Kityk R, Mayer MP. 2019. Hsp70- and Hsp90-mediated regulation of the conformation of p53 DNA binding domain and p53

cancer variants. Mol Cell. 74:831–843.e4. doi:10.1016/j.molcel.2019.03.032

Brachmann RK, Vidal M, Boeke JD. 1996. Dominant-negative p53 mutations selected in yeast hit cancer hot spots. Proc Natl Acad Sci U S A. 93:4091–4095. doi:10.1073/pnas.93.9.4091

Brown CR, McCann JA, Chiang H-L. 2000. The heat shock protein Ssa2p is required for import of fructose-1,6-bisphosphatase into vid vesicles. J Cell Biol. 150:65–76. doi:10.1083/jcb.150.1.65

Brownridge P, Lawless C, Payapilly AB, Lanthaler K, Holman SW, *et al.* 2013. Quantitative analysis of chaperone network throughput in budding yeast. Proteomics. 13:1276–1291. doi:10.1002/pmic.201200412

Bullock AN, Henckel J, DeDecker BS, Johnson CM, Nikolova PV, *et al.* 1997. Thermodynamic stability of wild-type and mutant p53 core domain. Proc Natl Acad Sci U S A. 94:14338–14342.

Bullock AN, Fersht AR. 2001. Rescuing the function of mutant p53. Nat Rev Cancer. 1:68–76. doi:10.1038/35094077

Cañadillas JMP, Tidow H, Freund SMV, Rutherford TJ, Ang HC, *et al.* 2006. Solution structure of p53 core domain: structural basis for its instability. Proc Natl Acad Sci U S A. 103:2109–2114. doi:10.1073/pnas.0510941103

Collins SR, Miller KM, Maas NL, Roguev A, Fillingham J, *et al.* 2007. Functional dissection of protein complexes involved in yeast chromosome biology using a genetic interaction map. Nature. 446:806–810. doi:10.1038/nature05649

Costanzo M, Baryshnikova A, Bellay J, Kim Y, Spear ED, *et al.* 2010. The genetic landscape of a cell. Science. 327:425–431. doi:10.1126/science.1180823

Davierwala AP, Haynes J, Li Z, Brost RL, Robinson MD, *et al.* 2005. The synthetic genetic interaction spectrum of essential genes. Nat Genet. 37:1147–1152. doi:10.1038/ng1640

Dearth LR, Qian H, Wang T, Baroni TE, Zeng J, *et al.* 2007. Inactive full-length p53 mutants lacking dominant wild-type p53 inhibition highlight loss of heterozygosity as an important aspect of p53 status in human cancers. Carcinogenesis. 28:289–298. doi:10.1093/carcin/bgl132

Dekker C, Stirling PC, McCormack EA, Filmore H, Paul A, *et al.* 2008. The interaction network of the chaperonin CCT. EMBO J. 27: 1827–1839. doi:10.1038/emboj.2008.108

Di Ventura B, Funaya C, Antony C, Knop M, Serrano L. 2008. Reconstitution of Mdm2-dependent post-translational modifications of p53 in yeast. PLoS One. 3:e1507.doi:10.1371/journal.pone.0001507

Escusa-Toret S, Vonk WIM, Frydman J. 2013. Spatial sequestration of misfolded proteins by a dynamic chaperone pathway enhances cellular fitness during stress. Nat Cell Biol. 15:1231–1243. doi:10.1038/ncb2838

Finnigan GC, Duvalyan A, Liao EN, Sargsyan A, Thorner J. 2016. Detection of protein-protein interactions at the septin collar in *Saccharomyces cerevisiae* using a tripartite split-GFP system. Mol Biol Cell. 27:2708–2725. doi:10.1091/mbc.E16-05-0337

Fourie AM, Hupp TR, Lane DP, Sang B-C, Barbosa MS, *et al.* 1997. HSP70 binding sites in the tumor suppressor protein p53. J Biol Chem. 272:19471–19479. doi:10.1074/jbc.272.31.19471

Gaglia G, Guan Y, Shah JV, Lahav G. 2013. Activation and control of p53 tetramerization in individual living cells. Proc Natl Acad Sci U S A. 110:15497–15501. doi:10.1073/pnas.1311126110

Gaglia G, Lahav G. 2014. Constant rate of p53 tetramerization in response to DNA damage controls the p53 response. Mol Syst Biol. 10:753.doi:10.15252/msb.20145168

Gautschi M, Mun A, Ross S, Rospert S. 2002. A functional chaperone triad on the yeast ribosome. Proc Natl Acad Sci U S A. 99: 4209–4214. doi:10.1073/pnas.062048599

Godon C, Coullet S, Baus B, Alonso B, Davin AH, *et al.* 2005. Quantitation of p53 nuclear relocation in response to stress using a yeast functional assay: effects of irradiation and modulation by heavy metal ions. Oncogene. 24:6459–6464. doi:10.1038/sj.onc.1208785

Green MR, Sambrook J. 2016. Precipitation of DNA with ethanol. Cold Spring Harb Protoc. 2016:pdb.prot093377.doi:10.1101/pdb.prot093377

Hainaut P, Butcher S, Milner J. 1995. Temperature sensitivity for conformation is an intrinsic property of wild-type p53. Br J Cancer. 71:227–231. doi:10.1038/bjc.1995.48

Hartwell LH. 1971. Genetic control of the cell division cycle in yeast. IV. Genes controlling bud emergence and cytokinesis. Exp Cell Res. 69:265–276.

Ho J, Tumkaya T, Aryal S, Choi H, Claridge-Chang A. 2019. Moving beyond P values: data analysis with estimation graphics. Nat Methods. 16:565–566. doi:10.1038/s41592-019-0470-3

Hu C-D, Chinenov Y, Kerppola TK. 2002. Visualization of interactions among bZIP and Rel family proteins in living cells using bimolecular fluorescence complementation. Mol Cell. 9:789–798. doi:10.1016/s1097-2765(02)00496-3

Huang P, Gautschi M, Walter W, Rospert S, Craig EA. 2005. The Hsp70 Ssz1 modulates the function of the ribosome-associated J-protein Zuo1. Nat Struct Mol Biol. 12:497–504. doi:10.1038/nsmb942

Huh W-K, Falvo JV, Gerke LC, Carroll AS, Howson RW, *et al.* 2003. Global analysis of protein localization in budding yeast. Nature. 425:686–691. doi:10.1038/nature02026

Inga A, Resnick MA. 2001. Novel human p53 mutations that are toxic to yeast can enhance transactivation of specific promoters and reactivate tumor p53 mutants. Oncogene. 20:3409–3419. doi:10.1038/sj.onc.1204457

Johnson CR, Weems AD, Brewer JM, Thorner J, McMurray MA. 2015. Cytosolic chaperones mediate quality control of higher-order septin assembly in budding yeast. Mol Biol Cell. 5:1323–1344. doi:10.1091/mbc.E14-11-1531

Johnson CR, Steingesser MG, Weems AD, Khan A, Gladfelter A, *et al.* 2020. Guanidine hydrochloride reactivates an ancient septin hetero-oligomer assembly pathway in budding yeast (A. Akhmanova, and M. Farkasovsky, Eds.). Elife. 9:e54355. doi:10.7554/eLife.54355

Kaganovich D, Kopito R, Frydman J. 2008. Misfolded proteins partition between two distinct quality control compartments. Nature. 454:1088–1095. doi:10.1038/nature07195

Kerppola TK. 2008. Bimolecular fluorescence complementation (BiFC) analysis as a probe of protein interactions in living cells. Annu Rev Biophys. 37:465–487. doi:10.1146/annurev.biophys.37.032807.125842

Kim Y, Jung JP, Pack C-G, Huh W-K. 2019. Global analysis of protein homomerization in *Saccharomyces cerevisiae*. Genome Res. 29:135–145. doi:10.1101/gr.231860.117

Krogan NJ, Cagney G, Yu H, Zhong G, Guo X, *et al.* 2006. Global landscape of protein complexes in the yeast *Saccharomyces cerevisiae*. Nature. 440:637–643. doi:10.1038/nature04670

Kuo Y-C, Lin Y-H, Chen H-I, Wang Y-Y, Chiou Y-W, *et al.* 2012. SEPT12 mutations cause male infertility with defective sperm annulus. Hum Mutat. 33:710–719. doi:10.1002/humu.22028

Leão M, Gomes S, Soares J, Bessa C, Maciel C, *et al.* 2013. Novel simplified yeast-based assays of regulators of p53-MDMX interaction and p53 transcriptional activity. FEBS J. 280:6498–6507. doi:10.1111/febs.12552

Liu S, Li J, Tao Y, Xiao X. 2007. Small heat shock protein alphaB-crystallin binds to p53 to sequester its translocation to mitochondria during hydrogen peroxide-induced apoptosis. Biochem Biophys Res Commun. 354:109–114. doi:10.1016/j.bbrc.2006.12.152

Llorca O, Smyth MG, Carrascosa JL, Willison KR, Radermacher M, *et al.* 1999. 3D reconstruction of the ATP-bound form of CCT reveals the asymmetric folding conformation of a type II chaperonin. Nat Struct Biol. 6:639–642. doi:10.1038/10689

Lopes-Pacheco M, Boinot C, Sabirzhanova I, Morales MM, Guggino WB, *et al.* 2015. Combination of correctors rescue ΔF508-CFTR by reducing its association with Hsp40 and Hsp27. J Biol Chem. 290:25636–25645. doi:10.1074/jbc.M115.671925

Magtanong L, Ho CH, Barker SL, Jiao W, Baryshnikova A, *et al.* 2011. Dosage suppression genetic interaction networks enhance functional wiring diagrams of the cell. Nat Biotechnol. 29:505–511. doi:10.1038/nbt.1855

Millson SH, Truman AW, King V, Prodromou C, Pearl LH, *et al.* 2005. A two-hybrid screen of the yeast proteome for Hsp90 interactors uncovers a novel Hsp90 chaperone requirement in the activity of a stress-activated mitogen-activated protein kinase, Slt2p (Mpk1p). Eukaryot Cell. 4:849–860. doi:10.1128/EC.4.5.849-860.2005

Morimoto RI. 1998. Regulation of the heat shock transcriptional response: cross talk between a family of heat shock factors, molecular chaperones, and negative regulators. Genes Dev. 12:3788–3796. doi:10.1101/gad.12.24.3788

Mostowy S, Cossart P. 2012. Septins: the fourth component of the cytoskeleton. Nat Rev Mol Cell Biol. 13:183–194. doi:10.1038/nrm3284

Müller L, Schaupp A, Walerych D, Wegele H, Buchner J. 2004. Hsp90 regulates the activity of wild type p53 under physiological and elevated temperatures. J Biol Chem. 279:48846–48854. doi:10.1074/jbc.M407687200

Ng DT, Walter P. 1994. Protein translocation across the endoplasmic reticulum. Curr Opin Cell Biol. 6:510–516.

Nicholls CD, McLure KG, Shields MA, Lee PWK. 2002. Biogenesis of p53 involves cotranslational dimerization of monomers and posttranslational dimerization of dimers. Implications on the dominant negative effect. J Biol Chem. 277:12937–12945. doi:10.1074/jbc.M108815200

North S, Pluquet O, Maurici D, El-Ghissassi F, Hainaut P. 2002. Restoration of wild-type conformation and activity of a temperature-sensitive mutant of p53 (p53(V272M)) by the cytoprotective aminothiol WR1065 in the esophageal cancer cell line TE-1. Mol Carcinog. 33:181–188. doi:10.1002/mc.10038

O'Brate A, Giannakakou P. 2003. The importance of p53 location: nuclear or cytoplasmic zip code? Drug Resist Updat. 6:313–322. doi:10.1016/j.drup.2003.10.004

Park K-W, Hahn J-S, Fan Q, Thiele DJ, Li L. 2006. De novo appearance and "strain" formation of yeast prion [PSI+] are regulated by the heat-shock transcription factor. Genetics. 173:35–47. doi:10.1534/genetics.105.054221

Park S-K, Park S, Pentek C, Liebman SW. 2021. Tumor suppressor protein p53 expressed in yeast can remain diffuse, form a prion, or form unstable liquid-like droplets. iScience. 24:102000.doi:10.1016/j.isci.2020.102000

Pittman AMC, Lage MD, Poltoratsky V, Vrana JD, Paiardini A, *et al.* 2012. Rapid profiling of disease alleles using a tunable reporter of protein misfolding. Genetics. 192:831–842. doi:10.1534/genetics.112.143750

Preissler S, Deuerling E. 2012. Ribosome-associated chaperones as key players in proteostasis. Trends Biochem Sci. 37:274–283. doi:10.1016/j.tibs.2012.03.002

Sahni N, Yi S, Taipale M, Fuxman Bass JI, Coulombe-Huntington J, *et al.* 2015. Widespread macromolecular interaction perturbations

in human genetic disorders. Cell. 161:647–660. doi:10.1016/j.cell.2015.04.013

Schaefer RM, Heasley LR, Odde DJ, McMurray MA. 2016. Kinetic partitioning during de novo septin filament assembly creates a critical G1 "window of opportunity" for mutant septin function. Cell Cycle. 2441–2453. 15: doi:10.1080/15384101.2016.1196304

Schindelin J, Arganda-Carreras I, Frise E, Kaynig V, Longair M, et al. 2012. Fiji: an open-source platform for biological-image analysis. Nat Methods. 9:676–682. doi:10.1038/nmeth.2019

Schirmer EC, Homann OR, Kowal AS, Lindquist S. 2004. Dominant gain-of-function mutations in Hsp104p reveal crucial roles for the middle region. Mol Biol Cell. 15:2061–2072. doi:10.1091/mbc.E02-08-0502

Sepehrnia B, Paz IB, Dasgupta G, Momand J. 1996. Heat shock protein 84 forms a complex with mutant p53 protein predominantly within a cytoplasmic compartment of the cell. J Biol Chem. 271:15084–15090. doi:10.1074/jbc.271.25.15084

Sharma D, Masison DC. 2011. Single methyl group determines prion propagation and protein degradation activities of yeast heat shock protein (Hsp)-70 chaperones Ssa1p and Ssa2p. Proc Natl Acad Sci U S A. 108:13665–13670. doi:10.1073/pnas.1107421108

Sharma V, Monti P, Fronza G, Inga A. 2016. Human transcription factors in yeast: the fruitful examples of P53 and NF-κB. FEMS Yeast Res. 16: fow083.doi:10.1093/femsyr/fow083

Shaulsky G, Goldfinger N, Ben-Ze'ev A, Rotter V. 1990. Nuclear accumulation of p53 protein is mediated by several nuclear localization signals and plays a role in tumorigenesis. Mol Cell Biol. 10:6565–6577. doi:10.1128/mcb.10.12.6565

Singh LR, Gupta S, Honig NH, Kraus JP, Kruger WD. 2010. Activation of mutant enzyme function in vivo by proteasome inhibitors and treatments that induce Hsp70. PLoS Genet. 6:e1000807.doi:10.1371/journal.pgen.1000807

Sopko R, Huang D, Preston N, Chua G, Papp B, et al. 2006. Mapping pathways and phenotypes by systematic gene overexpression. Mol Cell. 21:319–330. doi:10.1016/j.molcel.2005.12.011

Stein KC, Kriel A, Frydman J. 2019. Nascent polypeptide domain topology and elongation rate direct the cotranslational hierarchy of Hsp70 and TRiC/CCT. Mol Cell. 75:1117–1130.e5. doi:10.1016/j.molcel.2019.06.036

Stommel JM, Marchenko ND, Jimenez GS, Moll UM, Hope TJ, et al. 1999. A leucine-rich nuclear export signal in the p53 tetramerization domain: regulation of subcellular localization and p53 activity by NES masking. Embo J. 18:1660–1672. doi:10.1093/emboj/18.6.1660

Sung M-K, Lim G, Yi D-G, Chang YJ, Yang EB, et al. 2013. Genome-wide bimolecular fluorescence complementation analysis of SUMO interactome in yeast. Genome Res. 23:736–746. doi:10.1101/gr.148346.112

Trinidad AG, Muller PAJ, Cuellar J, Klejnot M, Nobis M, et al. 2013. Interaction of p53 with the CCT complex promotes protein folding and wild-type p53 activity. Mol Cell. 50:805–817. doi:10.1016/j.molcel.2013.05.002

Wang Y, Zhang X, Zhang H, Lu Y, Huang H, et al. 2012. Coiled-coil networking shapes cell molecular machinery. Mol Biol Cell. 23:3911–3922. doi:10.1091/mbc.E12-05-0396

Wang RY-R, Noddings CM, Kirschke E, Myasnikov AG, Johnson JL, et al. 2020. GR chaperone cycle mechanism revealed by cryo-EM: inactivation of GR by GR:Hsp90:Hsp70:Hop client-loading complex. bioRxiv doi:10.1101/2020.11.05.370247

Wawrzynow B, Zylicz A, Zylicz M. 2018. Chaperoning the guardian of the genome. The two-faced role of molecular chaperones in p53 tumor suppressor action. Biochim Biophys Acta Rev Cancer. 1869:161–174. doi:10.1016/j.bbcan.2017.12.004

Weems AD, Johnson CR, Argueso JL, McMurray MA. 2014. Higher-order septin assembly is driven by GTP-promoted conformational changes: evidence from unbiased mutational analysis in Saccharomyces cerevisiae. Genetics. 196:711–727. doi:10.1534/genetics.114.161182

Weems AD, McMurray MA. 2017. The step-wise pathway of septin hetero-octamer assembly in budding yeast. Elife. 6:e23689. doi:10.7554/eLife.23689

Werner-Washburne M, Stone DE, Craig EA. 1987. Complex interactions among members of an essential subfamily of hsp70 genes in Saccharomyces cerevisiae. Mol Cell Biol. 7:2568–2577. doi:10.1128/mcb.7.7.2568

Whitesell L, Sutphin PD, Pulcini EJ, Martinez JD, Cook PH. 1998. The physical association of multiple molecular chaperone proteins with mutant p53 is altered by geldanamycin, an hsp90-binding agent. Mol Cell Biol. 18:1517–1524. doi:10.1128/mcb.18.3.1517

Wiech M, Olszewski MB, Tracz-Gaszewska Z, Wawrzynow B, Zylicz M, et al. 2012. Molecular mechanism of mutant p53 stabilization: the role of HSP70 and MDM2. PLoS One. 7:e51426. doi:10.1371/journal.pone.0051426

Woods BL, Gladfelter AS. 2021. The state of the septin cytoskeleton from assembly to function. Curr Opin Cell Biol. 68:105–112. doi:10.1016/j.ceb.2020.10.007

Yam AY, Xia Y, Lin H-TJ, Burlingame A, Gerstein M, et al. 2008. Defining the TRiC/CCT interactome links chaperonin function to stabilization of newly made proteins with complex topologies. Nat Struct Mol Biol. 15:1255–1262. doi:10.1038/nsmb.1515

Zhang W, Guo XY, Hu GY, Liu WB, Shay JW, et al. 1994. A temperature-sensitive mutant of human p53. Embo J. 13:2535–2544.

Zhang Y, Sinning I, Rospert S. 2017. Two chaperones locked in an embrace: structure and function of the ribosome-associated complex RAC. Nat Struct Mol Biol. 24:611–619. doi:10.1038/nsmb.3435

Zhao R, Davey M, Hsu Y-C, Kaplanek P, Tong A, et al. 2005. Navigating the chaperone network: an integrative map of physical and genetic interactions mediated by the hsp90 chaperone. Cell. 120:715–727. doi:10.1016/j.cell.2004.12.024

Zylicz M, King FW, Wawrzynow A. 2001. Hsp70 interactions with the p53 tumour suppressor protein. Embo J. 20:4634–4638. doi:10.1093/emboj/20.17.4634

Communicating editor: C. Boone